Universidade de Aveiro
2021

Rui Pedro de Oliveira Vidal

Modelação numérica do fluido cefalorraquidiano cerebral

Numerical modelling of the cerebrospinal fluid

Universidade de Aveiro
2021

Rui Pedro de Oliveira Vidal

Modelação numérica do fluido cefalorraquidiano cerebral

Numerical modelling of the cerebrospinal fluid

Dissertação apresentada à Universidade de Aveiro para cumprimento dos requisitos necessários à obtenção do grau de Mestre em Engenharia Mecânica, realizada sob orientação científica do Doutor Ricardo José Alves de Sousa, Professor Auxiliar com Agregação do Departamento de Engenharia Mecânica da Universidade de Aveiro e de Doutor Fábio António Oliveira Fernandes, Investigador Auxiliar em regime laboral do Departamento de engenharia mecânica da Universidade de Aveiro.

Thesis presented to the University of Aveiro as a requirement to obtain the Master Degree in Mechanical Engineering, and carried out under the scientific supervision of Doctor Ricardo José Alves de Sousa, Assistant Professor at Department of Mechanical Engineering, University of Aveiro and Fábio António Oliveira Fernandes, Assistant Researcher at Department of Mechanical Engineering, University of Aveiro.

Esta dissertação teve o apoio financeiro dos projetos UIDB/004 81/2020 e UIDP/00481/2020 - Fundação para a Ciência e a Tecnologia; e CENTRO-01 -0145 FEDER-022083 - Programa Operacional Regional do Centro (Centro2020), através do Portugal 2020 e do Fundo Europeu de Desenvolvimento Regional.

O júri / The jury

Presidente / President	**Professor Doutor António Manuel de Amaral Monteiro Ramos** Professor Auxiliar, Universidade de Aveiro
Vogais / Committee	**Professor Doutor Ricardo José Alves de Sousa** Professor Auxiliar com Agregação, Universidade de Aveiro (Orientador)
	Professor Doutor Marco Paulo Lages Parente Professor Auxiliar, Faculdade de Engenharia da Universidade do Porto

Agradecimentos / Acknowledgements

To my parents and family for all the support.

Palavras-chave Liquido cefalorraquidiano, matéria dura, modelo de cabeça de elementos finitos

Resumo Os acidentes de viação apresentam-se ainda hoje em dia como um problema de grande relevância, visto que mais de 50 milhões de pessoas são feridas ou gravemente feridas todos os anos e, como consequência disto, os danos cerebrais representam impactos muito graves que precisam de ser avaliados. Os testes necessários para efectuar essa avaliação são de elevada complexidade em cadáveres e ilegais em individuos vivos. Neste sentido existe uma grande necessidade de desenvolvimento de modelos de elementos finitos da cabeça do ser humano não só para avaliar a resposta desta em impactos mas também para auxilio no design de equipamentos de protecção e segurança. Nesta dissertação um novo método de modelar o liquido cefalorraquidiano (*fluid cavity*) é implementado e validado contra dados experimentais. Este método tem a vantagem de facilitar a discritização do CSF e de resolver o problema de distorção de malha das técnicas actuais no entanto não traduz convenientemente a funcionalidade do mesmo o que leva a que ainda assim produza resultados menos precisos.

Keywords Cerebropsinal fluid, dura mater, finite element head model

Abstract Traffic accidents are still presented today as a problem of great relevance, as more than 50 million people are injured or seriously injured every year and, as a consequence of this, brain damage represents very serious impacts that need to be be evaluated. The tests needed to carry out this assessment are highly complex on cadavers and illegal on live individuals. In this sense, there is a great need to develop finite element models of the human being's head, not only to assess its response to impacts, but also to assist in the design of protection and safety equipment. In this dissertation a new method of modeling the cerebrospinal fluid (*fluid cavity*) is implemented and validated against experimental data. This method has the advantage of facilitating the description of the CSF and of solving the mesh distortion problem of current techniques, however it does not conveniently translate its functionality which leads to it still producing less accurate results.

Contents

List of Tables

List of Figures

List of Acronyms

BV	Bridging Veins
CT	Computed Tomography
FEHM	Finite Element Head Model
GCS	Glasgow Coma Scale
HIC	Head Injury Criteria
SDH	Subdural Haematoma
SI	Severity Index
SSS	Superior Sagittal Sinus
TBI	Traumatic Brain Injury
YEAHM	Yet Another Head Model
CNS	Central nervous system
PNS	Peripheral nervous system
CSF	Cerebrospinal fluid
RTA	Road traffic accidents
WHO	World health organization
FE	Finite element
DAI	Diffuse axonal injury
MRI	Magnetic ressonance imaging

List of Symbols

K_0	Bulk modulus
ρ	Density
ν	Poisson's ratio
N	polynomial order
G_0/G_∞	Shear modulus
U	Strain energy
σ	Stress
E	Young's modulus
β	Decay factor

Chapter 1

Introduction

In this chapter the motivation for the work developed is presented

1.1 Motivation

Road traffic accidents (RTA's) have been identified by several leading public health organizations as a major problem since in its report the World Health Organization(WHO) estimated that 1.2 million people die in those accidents and another 50 million are injured each year [11]. In the same report WHO states that if preventive measures are not implemented the tendency of RTA's number is to increase.

One of the severest consequences of RTA's is traumatic brain injuries. According to Arvind Kumar [1] in a study developed in New Delhi, India across 5 years (2001-2005) out of 2472 autopsies performed on victims of RTA's, 1699 (68,73 %) suffered head injuries. Skull fractures were present in 1183 cases (69,63 %) being the temporal bone the most commonly fractured.

The study went further in detailing the type of injuries suffered alleging that in 72,53% of the cases with intracranial hemorrhage skull fracture was also present; the most ordinary hemorrhage was subdural hemorrhage and the least common was intracerebral hemorrhage. The pattern of cranial trauma can be observed in more detail in the following table 1.1.

Having in consideration that head trauma represents a big portion of the injuries caused by RTA's and that some internal bio-mechanical responses are difficult to be measured in cadavers and impossible in-vivo there is a need to develop Finite Element Head Models (FEHM), which are a cost-effective way to predict head injuries under external loads [8].

In order to achieve trustworthy results the finite element (FE) model has to be as realistic as possible therefore over the years many FEHM have been developed by different authors such as Fernandes [9], Hardy and Marcal [12], Kenner and Goldsmith [13] to

Table 1.1: Type of head injuries and their incidence - Retrieved from [1]

Injury	**No.**	**%**
Head injury	1699	68,79
Skull fracture	1183	69,63
Intracranial haemorrhage		
Subdural	1514	89,11
Subarachnoid	1240	72,98
Intracerebral	282	16,60
Extradural	344	20,25
Brain laceration	272	16,01

name a few.

After some literature review, we came to understand that most FEHM modeled the cerebrospinal fluid (CSF) as a solid (elastic or viscoelastic material) and then changed its mechanical properties like Bulk modulus to make it act like a fluid.

Even though this is a good approximation and computationally efficient, depending on the impact tests performed it tends to make results somewhat inaccurate due to severe mesh distortions. In cases of CSF modelled as an elastic material, the coup pressure (the pressure measured under the impact location) increased while contrecoup pressure (the pressure measured at the opposite side from the impact location) decreased in purely translational impacts.

With the view to keep evolving Fernandes [9] FEHM and make it produce trustworthier results the objective of this dissertation is to test a new method of modelling the CSF.

1.2 Reading Guide

The present work is split in 5 chapters, a brief summary of each is presented below.

Chapter 1 - Introduction: in this chapter a motivation for this thesis as well as a summary of the content present in each chapter.

Chapter 2 - State-of-the-art: this chapter contains an overview of the human head and its constituent parts, reviews the types of head traumas and methods to assess their severity, finally FEHMs are thoroughly reviewed including their history, material models and boundary conditions used.

Chapter 3 - Methodology: in this chapter the method used to model the new CSF geometry, the material models and the validation methodology used is presented.

Chapter 4 - Simulation and results: the simulations results are presented and analysed in this chapter.

Chapter 5 - Conclusions and future works: in this chapter the results obtained along the present work are discussed and also some opinions on what the future work might be are woven.

Chapter 2

State-of-the-art

This chapter addresses matters relative to the human head, its components and finite element head models and their respective properties.

2.1 Head anatomy

The human head is one of the most important parts of the body since it contains the brain and it is essential to control the body, all of our human senses such as hearing, sight, smell, and taste but also the most vulnerable in case of external loads from RTA, violence, and others.

These injuries have an important role due to their severity and thus as referred before, many experiments have taken place throughout history and with many authors using different methods from cadaver heads, animal heads, physical head models to in vitro.

In this state of the art, the different parts of the brain will be studied in order to have a good understanding of them and their characteristics focusing particularly on the CSF. FEHM's will also be reviewed.

2.2 Nervous System

The nervous system can be defined as a collection of nerves and cells (neurons) that emit electric signals. To simply put it, it can be expressed as the body's electrical wiring; it is equipped with sense organs (receptors) making it able to extract the information received, store the parts needed and send out commands to muscles or glands if and when necessary [14].

This system is structurally divided into two parts: the central nervous system and the peripheral nervous system [15], has the main task of defining the human being since it enables thought, learning, and memory but also regulates human behaviour according to the brain's interpretation of reality [16].

The Peripheral nervous system (PNS) is composed of nerves some denominated cranial nerves coming from the brain and others called spinal nerves which emerge from the spinal cord. The function of this system is to send neural messages from the sense organs to the central nervous system and from the former to the glands and muscles of the body [14].

As stated by [16] the building block of the Central Nervous System (CNS) is the neuron and there are billions of them forming an intricate network for communicating and information processing.

The CNS is mainly composed by two parts: the brain and the spinal chord. The brain itself can be further divided into four major regions being them: Cerebrum, Diencephalon, Brain Stem and the Cerebellum whereas the spinal cord can be considered a single structure [17]. An illustration of the central and peripheral nervous systems and the spinal cord can be seen in figure 2.1

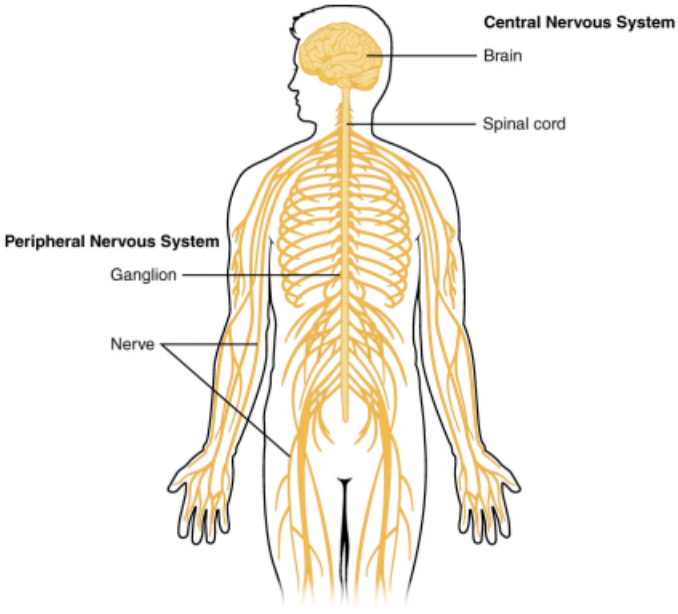

Figure 2.1: Illustration of the central and peripheral nervous systems - Retrieved from [17]

2.2.1 Cerebrum

The Cerebrum can be described as having an egg-like shape, occupies a large percentage of the cranial cavity [16] and is protected by the scalp, skull and meninges [18].

The cerebrum is composed of two types of tissues called grey and white matter. Grey matter is the outer layer of the cerebrum and is called the cerebral cortex while white matter is the inner layer. Grey matter is the major responsible for consciousness and has the unique characteristic of being folded forming the so-called sulci and gyri which are

the valleys and the hills, respectively. Sulci and gyri are an important feature due to the fact that being this way allows for more cerebral cortex to fit inside the cranial cavity [19].

From a structural standpoint the cerebrum can be divided in two hemispheres, left and right and connecting them is the corpus callossum which is a pathway that enables communication between the two hemispheres [17; 20]. From a functional point of view it can be divided into lobes being them: Frontal, Parietal, Occipital and temporal which are named after the skull bone they are under and can be seen in figure 2.2.

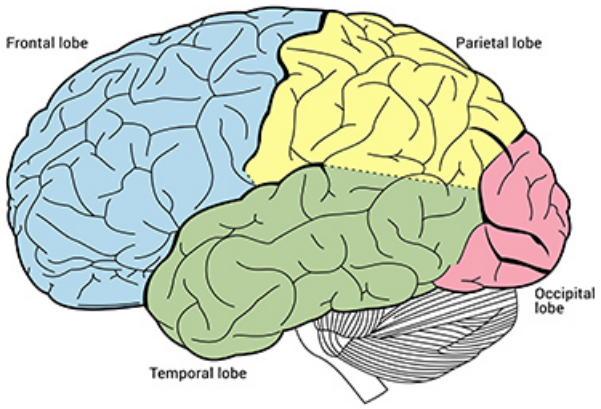

Figure 2.2: Brain lobes and their location within the brain structure - Retrieved from [19]

Frontal Lobe

Frontal lobes are positioned at the front of each brain hemisphere and are separated from the parietal lobe by a fissure denominated by "*central sulcus*" and from the parietal lobes by the "*lateral sulcus*" [21] and can be seen in blue in figure 2.2.

This lobe is the largest when compared to the frontal lobes of other primates [22] and is associated with functions of motor planning, motor output, expressive language and higher-level executive functions such as: the capacity to plan, organisation, initiating ideas, self-monitor and accomplish goals [21; 22].

Parietal Lobe

The Parietal lobes lie behind the frontal lobe, in front of the Occipital lobe [21] and above the temporal lobe [23]. This lobe can be seen in yellow in figure 2.2.

This lobe is mainly known for holding the somatosensory cortex; has 5 main functions, one of them is the somatic sensation that translates to touch sensation, limbs position, and temperature monitoring; the second is space analysis using sensory information; the third is to send commands to the motor system; the fourth is an important one since

it generates attention and the fifth and last of the major functions are visual motion analysis [22; 23].

Occipital Lobe

This lobe is positioned behind the Parietal Lobe and above the cerebellum in the very posterior region of the brain; this lobe occupies 10 % of the brains mass [24] and can be seen in pink colour in image 2.2.

The visual cortex is located [22] in this lobe and its main function is to receive visual information from the eyes and then send that information to other processing areas in order to get informations like: depth, distance, location and identity of objects [21] and also interpretation of colours, light and movement [18].

Temporal Lobe

The temporal lobe is located below the Frontal and Parietal lobes and is separated from the first by the lateral fissure [21] and can be seen in figure 2.2 in green.

This lobe is where the speech and language systems are located and is mainly known for sound and language processing [22] but that is not all it does. The temporal lobe also is important in functions such as memory, organising and sequencing tasks [18; 21]

2.2.2 Diencephalon

The Diencephalon is divided into 4 main parts that are: the thalamus, subthalamus, hypothalamus and epithalamus although its two major parts are the thalamus and hypothalamus.

In the following image 2.3 Diencephalon location can be observed as well as its main parts.

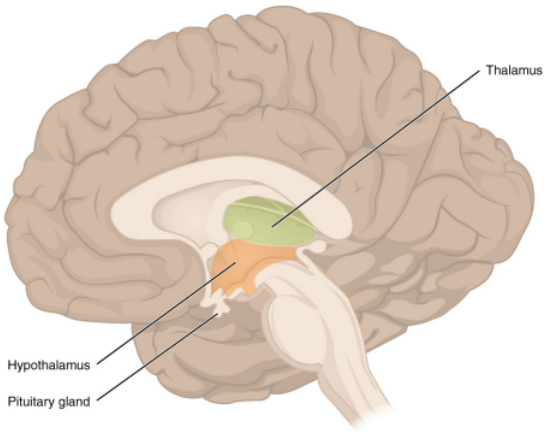

Figure 2.3: Representation of the Thalamus, Hypothalamus and the Pituitary gland - Retrieved from [17]

Hypothalamus main function is to link the nervous system to the endocrine system via the pituitary gland but has also the purpose of regulating temperature and deal with metabolic processes; thalamus performs a variety of functions including vigilance, sleep, controlling consciousness, broadcasting motor signals and sensory information to the cerebral cortex; subthalamus possesses numerous connections to different parts of the brain such as the "*substantia negra*" ; epithalamus is located at the posterior segment of the diencephalon and its primary function is the segregation of melatonin [25].

The diencephalon can be thought of as a connection between the Cerebrum and the rest of the Nervous system, every output from the cerebrum is passed on through the diencephalon except the olfactory information which goes directly to the cerebrum without having to pass through the diencephalon; this part of the brain is located below the cerebrum and constitutes the walls of the third ventricle [17].

2.2.3 Brain Stem

The Brainstem is composed of three different parts which are: the midbrain, the pons and the medulla oblongata; the function of this part of the brain is to connect the forebrain (cerebrum and diencephalon) with the spinal cord.

In the image presented below 2.4 an illustration of the brainstem, the different parts, and its position in the brain can be seen in detail. Basilar artery and vertebral arteries are also present.

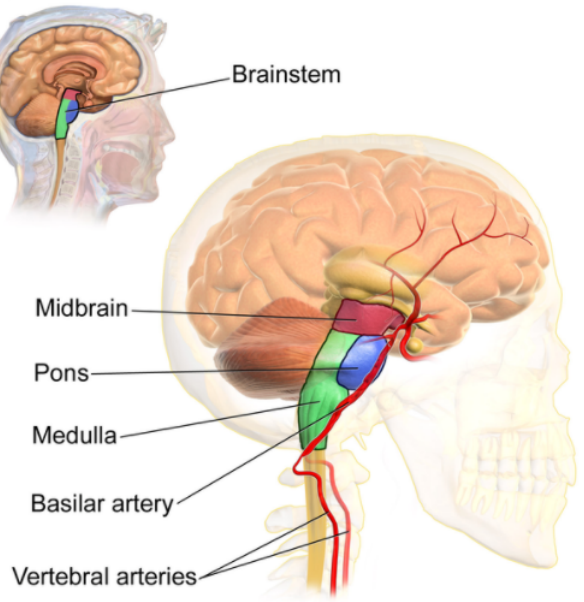

Figure 2.4: Visual representation of the elements that compose the Brainstem - Retrieved from [25]

Mid Brain constitutes the shortest part of the brainstem and is the part that connects the

pons to the diencephalon. This part of the brain also forms what is called the "*Sylvius aqueduct*" and connects the third and fourth ventricles.

Pons is a transverse voluminous mass that connects the midbrain and the medulla, in addition at either end they form a bridge between the two hemispheres justifying that way its name.

The Medulla oblongata is a continuation of the spinal cord and goes from the "*foramen magnum*" to the top border of the pons. The lower part contains the central canal which is a closed region while the upper parts is a widened canal that forms the lower part of the fourth ventricle [26].

Although its primary function is to connect the cerebrum to the spinal cord, brainstem also has other important functions as regulating heart and breathing rate, regulating sleep, send body nerve and sensory information to the cerebrum and cerebellum [25].

2.2.4 Cerebellum

Cerebellum, also called "*the little brain*", resembles a fist because of its geometry; is covered in gyri and sulci, has two hemispheres, and is composed of an outer layer of grey matter (cerebral cortex) and an inner layer of white matter, just as the cerebrum, and because of that they have a high degree of similarity in terms of appearance and composition [17; 27].

This part of the brain which is located at the back of the head, is connected anteriorly with the brainstem and performs important roles in controlling voluntary movement, maintaining posture, balance and although it does not initiate movements contributes with more accuracy in those.

Many studies also suggest that it is also involved in: cognitive functions as attention, language and controlling body responses to situations of fear and pleasure [28].

In the image below (2.5) we can view the Cerebellum position in the human head and examine its similarities in terms of shape.

2.2.5 Spinal cord

The spinal cord is attached to the brainstem (medulla oblongata - figure 2.6), can be defined as a cylinder of nervous tissues that extends from the bottom of the brainstem along the spine until the upper part of the second lumbar vertebra and is somewhat a highway of information between the brain (Cerebrum) and the body [29]; this part of the brain is whitish due to the presence of axons and has a soft, jellylike consistency [16].

The spinal cord has three main functions. The first and foremost are motor functions which is the action of transmitting information to produce voluntary movements, secondly are sensory functions which translates to supervising pain, touch, pressure and temperature senses, last but not least is autonomic functions such as urinating, controlling body

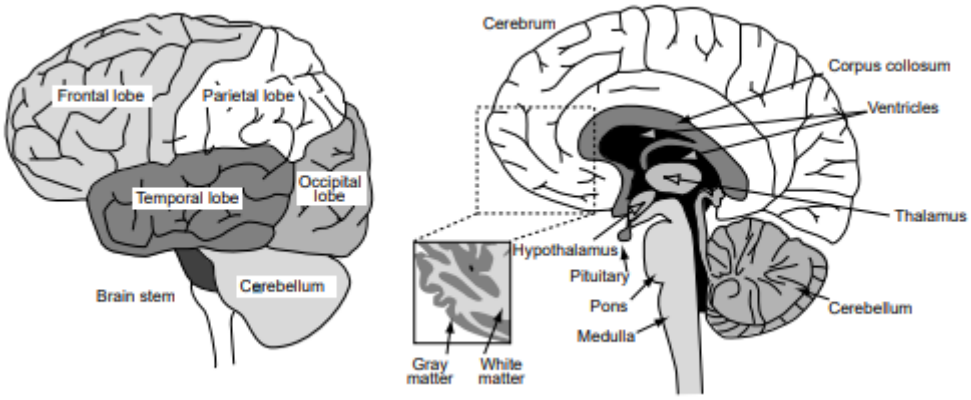

Figure 2.5: The location of the cerebellum can be seen in the image on the left and a cross section view on the image on the right - Retrieved from [27]

temperature, heart rate and adjusting blood pressure [29].

2.2.6 Cerebrospinal fluid

The human brain is surrounded by several layers that are called the meninges. The meninges are composed of three layers: dura matter which is the outer layer, an intermediate layer called arachnoid matter and an inner layer called pia matter. Between the arachnoid matter and the pia matter there is a space called arachnoid space where a fluid called Cerebrospinal fluid (CSF) circulates [16].

The Cerebrospinal fluid is a clear and colourless fluid, similar to blood plasma and interstitial fluid [26] that surrounds the brain and the spinal cord [3]. This fluid is composed mainly of water but also of: protein, gases (as oxygen and carbon dioxide), sodium, potassium, magnesium, chloride ions, glucose and white cells [14].

According to the literature, this fluid has 2 functions [14]:

1. Provides physical support - Surrounds the brain and contributes to buoyancy making the brain float and cushions the brain against impacts.

2. Homeostasis - Maintains the chemical equilibrium of the neural environment.

An interesting fact is that as the brain is immersed in CSF and has a net average weight of 1400 g it only weights 25 g because of the impulsion created by the CSF which makes the brain able to withstand fast impacts [14].

CSF is produced mostly in the lateral ventricles from their choroid plexus, passes the interventricular foramina "*of Monro*" but is also produced in the third and fourth ventricle by their respective choroid plexus[26].

The method of production of this fluid is still uncertain and the average human yields about 500 ml per day [14; 26] and the total existing volume in a human is 150 ml, 60 ml

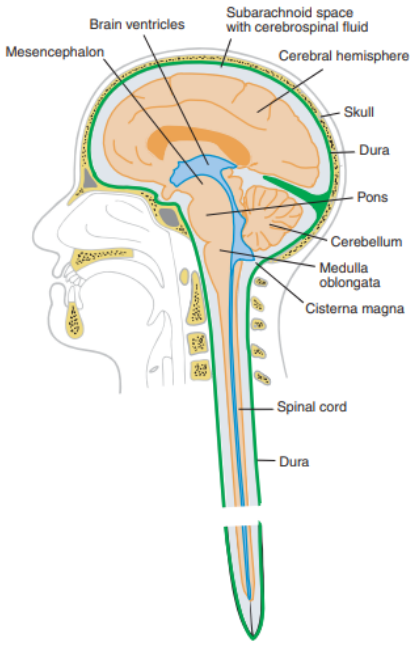

Figure 2.6: Spinal cord illustration - Retrieved from [16]

of those are in the ventricles and 90 ml in the subarachnoid space [14].

CSF volume is replaced every day, several times, being renewed and reabsorbed in a way that the total volume maintains constant [14].

The structures responsible for renewing and absorbing are [14]:

- The brain capillaries
- Choroid plexus

If an accumulation of CSF happens there can be two types of injuries: internal hydrocephalus and/or external hydrocephalus. If the accumulation happens within the ventricular system this is then called internal hydrocephalus and can happen due to a blockage of the choroid plexus or the exit through the foramina in the fourth ventricle; on the other hand, if the accumulation happens in the sub arachnoid space (figure 2.7) this condition is called external hydrocephalus. Specifically, this type of injury happens typically due to a blockage of the "*arachnoid villi*" and granulation. [26].

Ventricular system

Ventricles are open spaces inside the brain where CSF circulates aiming to remove metabolic wastes from the nervous tissues to the bloodstream. The first two ventricles are the lateral ones and these open spaces are located in the cerebrum, then there is the third located between both sides of the diencephalon and the fourth located between the pons/upper medulla and the cerebellum [17]. In figure 2.8 the ventricular system and its

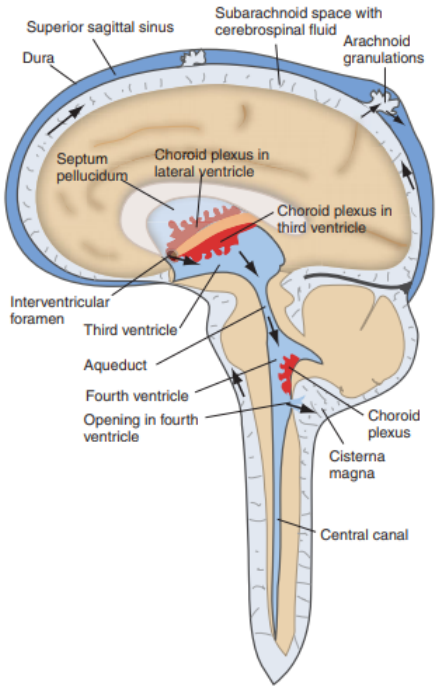

Figure 2.7: Sub arachnoid space filled with cerebrospinal fluid - Retrieved from [16]

structures can be seen in detail.

The ventricles are connected to each other allowing CSF to circulate through. The lateral ventricles are connected to the third ventricle through what is called the inter-ventricular foramina, then the latter (third ventricle) is connected to the fourth through the cerebral aqueduct [17].

The CSF circulations occur from the lateral ventricles (where it is produced) to the third ventricle, then through the cerebral aqueduct into the fourth ventricle. After arriving at the fourth ventricle the major part of this fluid flows into the sub arachnoid space and a minor part down the central canal of the spinal cord bathing all parts of the central nervous system [17] being then resorbed by arachnoid granulations [31].

One important thing to note is that the flow of the CSF is not laminar and unidirectional but rather pulsating and bidirectional [31].

Cerebrospinal fluid modelling properties

Throughout the years many authors have been developing head models to accurately predict head injuries such as traumatic brain injuries (TBI's). But the model is only as accurate as the boundary conditions BC's applied and as the material properties used to prescribe the model. Since the CSF acts as a damper against head motion it has a critical role in head impacts so it is important to meticulously model CSF to achieve good results in head injury simulations. One common way to model CSF is modelling it as a layer of bricks assumed to be linear elastic with a Young modulus of 12 kPa and a

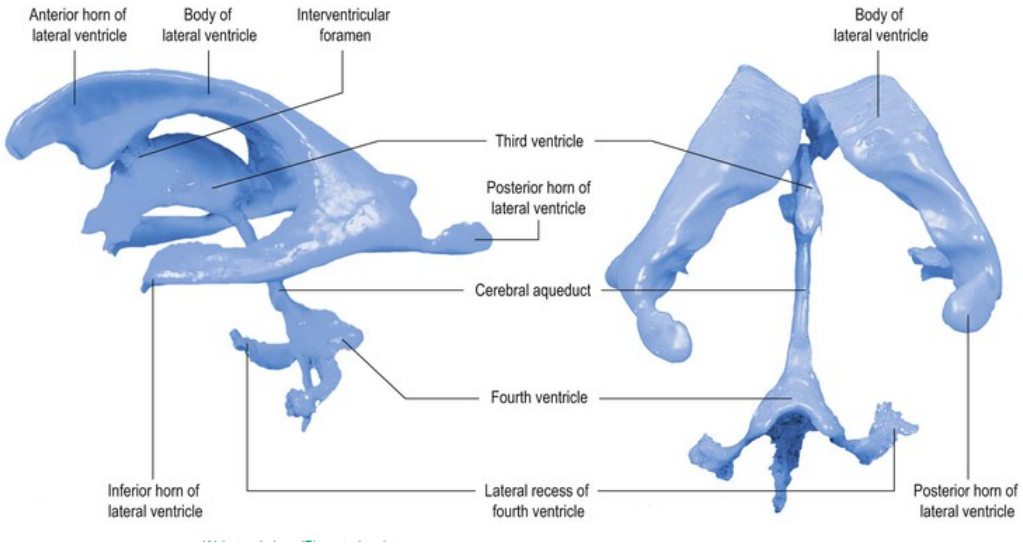

Figure 2.8: Constituent parts of the ventricular system - Adapted from [30]

Table 2.1: Material definition and respective property values used - Adapted from [2]

Material definition	**Property values**	**Reference**
Fluid 1	K = 1,65 MPa	Ruan [32]
Fluid 2	K = 22 MPa	Zhou, Chen, Yan [33]
Fluid 3	K = 100 MPa	Choi [34]
Fluid 4	K = 2,1 GPa	Willinger [35]
Elastic 1	E = 12kPa	Willinger [35]
Elastic 2	E = 0,15 MPa	Horgan [36]
Elastic 3	E = 2,19 MPa	Zong [37]
Viscoelastic 1	$G_0 = 407$ Pa, $G_\infty = 233$ Pa, $\beta = 80\ s^{-1}$	Mao [38]
Viscoelastic 2	$G_0 = 1000$ Pa, $G_\infty = 900$ Pa, $\beta = 80\ s^{-1}$	Yang [39]

Poisson ratio close to 0,5 (incompressible fluid) [2].

Jin [2] carried out a study on the effects of the modelling properties of CSF in FEHM using for effect different methods namely: elastic, fluid and viscoelastic and also tested different values of certain properties which can be seen in the table presented below. After that, the simulation values were compared to experimental data of different authors.

From the simulations the conclusions drawn were:

- The best results occurred when CSF was modelled as a fluid with a bulk modulus of 2,19 GPa having the best correlation with experimental data.
- When CSF was modelled as fluid the coup pressure (the pressure under the point of impact) increased while the countrecoup pressure (pressure on the opposite side of the point of impact) decreased when the head suffered purely translational impacts. It also states that if an increased bulk modulus was used the coup, countrecoup and skull-brain relative motion decreased under rotational impacts.
- CSF modelled as an elastic material produced increased coup pressure and a decreased countrecoup pressure with increased bulk modulus under pure translational impacts. To notice that these results didn't follow the same trend under rotation.
- In cases where CSF was modelled as an elastic material the model tended to underestimate brain injuries during pure translational impacts.
- CSF modelled as a fluid and with a high bulk modulus is the most appropriate to model CSF and to predict the brain response during impacts to the head.

Another study worth referring is the study of Chaf [3] that executed a similar study to the previously mentioned. This author modelled the CSF in three different ways:

1. CSF modelled as an elastic material with fluid-like properties;
2. CSF modelled as a viscoelastic material;
3. CSF modelled as an elastic material with Poisson coefficient of 0,5 (incompressible fluid) with a low shear modulus and high bulk modulus

The properties values used to model each case described above are presented below.

Table 2.2: Material properties used for CSF modelled as an elastic material with fluid-like properties - Adapted from [3]

Case study	**Density** ρ $[Ton/mm^3]$	**Bulk modulus** K [MPa]	**Poisson's ratio** $[\nu]$	**Viscosity Coefficient** [VC]
1	$1,04 \times 10^{-9}$	219	0,5	0,2
2	$1,04 \times 10^{-9}$	21,9	0,5	0,2
3	$1,04 \times 10^{-9}$	2,19	0,5	0,2
4	$1,04 \times 10^{-9}$	2,19	0,5	0,05

Table 2.3: Material properties used for CSF modelled as a viscoelastic material - Adapted from [3]

Case study	**Density** ρ $[Ton/mm^3]$	**Bulk modulus** K [MPa]	**Short term shear modulus** [Pa]	**Decay factor** [m/s]
1	$1,04 \times 10^{-9}$	219	500	500
2	$1,04 \times 10^{-9}$	21,9	500	500
3	$1,04 \times 10^{-9}$	2,19	500	500
4	$1,04 \times 10^{-9}$	2,19	5000	500

Table 2.4: Material characteristics used to model the CSF as a nearly incompressible elastic - Retrieved from [3]

Case study	**Density** [ρ Kg/mm^3]	**Shear modulus** [GPa]	**Bulk modulus** K [GPa]
1	1,0x10e-6	500	0,219
2	1,0x10e-6	500	0,0219
3	1,0x10e-6	500	0,00219
4	1,0x10e-6	5000	0,00219

And then, like the previous, the results of this simulation were compared to experimental data. Once again, and in accordance with the study carried out by JIN [2], the best results were produced when the CSF was modelled as a fluid-like material. Apart from the method used to model CSF (elastic, viscoelastic or fluid), this study states that the bulk modulus has a heavy impact on the skull-brain displacement. The study also concludes:

- CSF constitutive properties don't affect substantially the peak intracranial pressure. Nonetheless the brain strains and brain's local motion were considerable.
- When CSF was modelled with fluid-like properties the bulk modulus impact was negligible in terms of coupe peak pressure. However, it had a significant proportional impact on peak principal and shear strains and the highest inverse proportional impact on skull-brain relative motion. It was also found that the viscosity doesn't significantly affect the brain displacement.
- When CSF was modelled as a viscoelastic material the bulk modulus doesn't produce appreciable impact on the coup pressure and the bulk modulus had the highest impact on the skull-brain displacement but also that local brain motion, coup pressures and strains are insensible to shear modulus changes.
- When CSF was modelled as an nearly incompressible material the bulk modulus had a residual effect on the peak coup pressure. Nonetheless it had a significant impact on principal and shear strains although strain didn't show to be proportional to varying bulk modulus. Also it was found that shear modulus has an important impact on: peak, principal and shear strains and skull-brain relative motion but not on peak coup pressure.

2.3 Head injuries

Head injuries are every injury done to the brain, skull or scalp. A head injury can either be open or closed. An open head injury is one where the skull is broken and an open pathway to the brain is produced while a closed head injury is one where the skull is not fractured although a traumatic brain injury can occur.

Head injuries are hard to assess and there are many methods to classify them; common head injuries include: concussion, scalp wounds and skull fractures.

2.3.1 Traumatic brain injuries

TBI's can be defined as the consequences of the impact of an external force on the brain. This force can be of all kinds from mechanical forces to thermal, electrical, radiation, among others, and produces alterations in brain functions [40].

There are several different ways to tell apart different types of TBI's although in broad terms they can happen in one of two ways: one of them being closed and the other an open head injury and as the name implies in an open head injury the skull fractures and on a closed head injury the skull is not broken. TBI's can also be divided into primary and secondary head injuries (figure 2.9). The primary head injuries are the ones that happen immediately after the impact and can include injuries as scalp laceration, skull fracture, cerebral contusions among others. Secondary brain injuries can be characterised as delayed head injuries since they only appear after the impact and can include injuries as: Ischemia, hypoxia, cerebral swelling, among others [41].

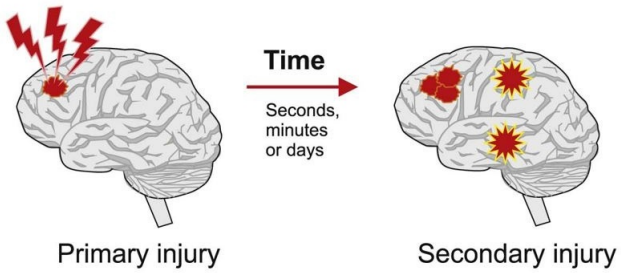

Figure 2.9: Primary and secondary injury types - retrieved from [42]

Although these two methods of classification are good first approaches a more specific way of describing a TBI is needed, therefore in clinical practice 3 main systems of classification are used [43]:

- Classification by injury severity.
- Classification Pathoanatomic.
- Physical mechanism.

Classification by severity

Another way to classify TBI's is through their severity. In this type of classification, the severity of the injury is assessed through scales. One of them is the Glasgow coma scale (GSC) and is used by health technicians to assess the degree of severity of a head impact which according to this scale can vary from mild to moderate and severe [43].

The GSC checks 3 areas of functioning namely eye movement, motor response and verbal response. According to the response of the patient a score is assigned. Then the score obtained by the patient in the 3 different areas evaluated is added, a final score is obtained

Table 2.6: Classification of the severity of a TBI through the Glasgow coma scale and the loss of conscious - Adapted from [4]

Severity	**GCS**	**Loss of consciousness**
Mild	13-5	$<$ 20 min to 1 hour
Moderate	9-12	1 hour to 24 hours
Severe	3-8	$>$ 24 hours

and according to the number that results the severity is classified. If the final score obtained is between 3-8 the injury is classified as severe, if the score is comprised between 9-12 then the injury is moderate, for an injury to be classified as mild the score has to be between 13-15 (table 2.6) [5].

Table 2.5: Glasgow coma scale punctuation system - Adapted from [5]

Eye opening	
Spontaneous	4
To speech	3
To pain	2
None	1
Best verbal response	
Oriented	5
Confused conversation	4
Inappropriate words	3
Incomprehensible sounds	2
None	1
Best motor response	
Obeys commands	6
Localises pain	5
Withdrawal (normal flexion)	4
Abnormal flexion (decorticate)	3
Extension (deceberate)	2
None	1

In addition to the GSC, another method used to estimate the severity of a head injury is the time duration of loss of consciousness. In this scale, if the duration of loss of consciousness is under 1 hour then it is classified as mild, if the loss of consciousness lasts between 1 hour to 24 hours it is considered moderate and a severe head injury is when the loss of consciousness lasts more than 24 hours [4].

Classification Pathoanatomic

The pathoanatomic classification is based on the description. It describes the location, its extent, multiplicity and distribution or the anatomical appearance of the injury. In this method of classification, a patient can have more than one type of injury and this technique of injury classification has evolved quite a bit since imaging became a standard

procedure in patients with head traumas [43].

In order to estimate the severity of the injury in this classification, the Rotterdam computed tomography score system is used. This system was developed in 2005 by Maas [44] and evaluates 4 fields of interest: the basal cisterns, midline shifts, presence of epidural mass lesions and the existence of intraventricular blood or traumatic subarachnoid haemorrhage [6]. The score assigned to each field can be seen in detail in the table below.

Table 2.7: Rotterdam score system - Adapted from [6]

Rotterdam score element	
Basal cisterns	
Normal	0
Compressed	1
Absent	2
Midline shift	
No shift or $\leq$ 5 mm	0
Shift $>$ 5 mm	1
Epidural mass lesion	
Present	0
Absent	1
Intraventricular blood or trauma subarachnoid hemorrhage	
Absent	0
Present	1
Sum score	**+1**

Classification by Physical Method

The physical mechanism of injury predicts injuries by analysing forces magnitude, checking whether the head hit an object or the object hit the head, brain and skull relative motion and the direction of the forces applied to estimate the severity of a head injury. Although this method has a good utility in clinical practice the conditions of the impact have to be estimated after the impact from partial details of the accident thus the severity of the head injury has to be predicted through a combination of physical mechanism and pathoanatomic findings [43].

2.4 Types of TBI's

Traumatic brain injuries have several types and can often coexist. Generally, they can be divided into two distinct groups: Diffuse and focal brain injuries being the difference between them the area affected by the injury. This classification is graphically explained in the figure 2.10 and will be briefly explained in the following chapters.

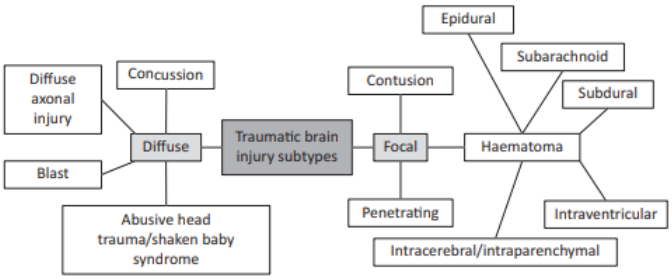

Figure 2.10: Subtypes of traumatic brain injuries - Adapted from [45]

2.4.1 Diffuse traumatic brain injuries

Diffuse axonal brain injury

Diffuse axonal injury (DAI) is widespread damage to the axons present in the white matter, brainstem, parasagittal white matter of the cerebral cortex, corpus callossum and the grey-white matter junctions of the cerebral cortex [46].

Concussion

It is defined as a process induced by mechanical forces that result in a transient neurologic dysfunction in which a patient recovers in a variable period of time; this neurologic dysfunction can result in loss of consciousness [47].

Blast

Blast head injuries are the injuries that result from a pressure wave generated for example by an explosion. The energy from the explosion is transformed into biokinetic energy causing damage to the brain and the structures of the skull from the overpressure. The damage produced by this type of injury is similar to a blunt TBI [48].

Abusive head trauma/shaken baby syndrome

This type of injury is more prevalent in infants and young children due to their soft brains and weak neck muscles. This injury as the name implies is caused by shaking a baby head causing their brain to violently hit the inside of the skull producing consequences such as cerebral oedema, retinal haemorrhage and subdural haematoma [49].

2.4.2 Focal brain injuries

Intracranial Haematomas

Intracranial haematomas are a rupture of a blood vessel producing an accumulation of blood in brain tissues and/or empty spaces in the brain. There are several different types of haematomas:

- Epidural haematoma: Blood clots formed between the skull and the dura matter.

- Subdural haematoma: Blood clot formed between the dura matter and the brain.
- Subarachnoid haemorrhage: Bleeding in the subarachnoid space between the dura matter and the space under the arachnoid matter.
- Intracerebral haematoma: Bleeding inside the brain itself due to the rupture of a blood vessel.
- Intraventricular haemorrhage: Bleeding into the ventricles of the brain.

Contussion

"Contusions are focal injuries that occur at locations where brain tissue comes in contact with irregular bony protuberances of the skull base, most often the inferior aspect of the frontal lobes, the frontal poles and the inferior aspect of the temporal lobes. Contusions result from damage to small blood vessels and other components of the brain parenchyma that produce small haemorrhages perpendicular to the cortical surface" [50].

Penetrating

Penetrating brain injuries also called open head injury is when an object penetrates the skull leaving the head open such as when a bullet pierces through the brain.

2.5 Existing FEM Head models

Head injuries have a high socioeconomic cost and most of all continue to be one major health problem. Performing impact tests on live human beings is illegal and extracting information from the deeper parts of the brain in cadavers can be especially hard due to change in the tissues material properties and the mechanical part of introducing sensors on those parts of the head in order to get that information, so there is a need to develop studies on the biomechanics of head impacts and its tolerance to external loading. In this sense the FEHMs presents as a cost-effective alternative to experimental testing.

Although experimental tests on cadavers are hard it didn't prevent several researchers from doing it and with great success. This type of experimentation started in the early 1900's and involved mostly the cerebrum and not the whole assembly [51]. These experiments are so important that they are still being used to this day as a way of validating notable FEHM's.

The first FEHM was developed by Hardy and Marcal [12], was a 2D model, consisting of the skull only and was later improved by [52] with the introduction of an elastic fluid-filled brain attached to the skull. The early 3D FEHM's were highly simplistic, using regular geometries such as spheres and ellipses and highly unrealistic in large deformations due to the lack of computational capability but then the '90s came along and with them the computational capability necessary to design more realistic models.

The first realistic model developed was the model created by Ruan [53] from the Wayne state university and was composed of skull, brain, CSF modelled with eight-noded hexahedron elements and scalp, dura matter, falx cerebri were modelled with four-noded shell elements.

The same model was improved in 1995 by Zhou [33] which differentiated grey and white matter and also incorporated the ventricles of the brain; then in 2001 Zhang [54] introduced the sliding interface between the skull and the brain which made it possible to achieve more precise results and details about the heterogeneity of the brain structures [7].

Ultimately this model was completely revised by King [39] this time including the scalp, a three-layered skull, dura, falx cerebri, tentorium, pia matter, CSF hemispheres, cerebrum, cerebellum, ventricles, brainstem and the facial bones.

In the final version, this model counted with 281800 nodes and 314500 elements defining the anatomical features of a 50^{th} percentile male.

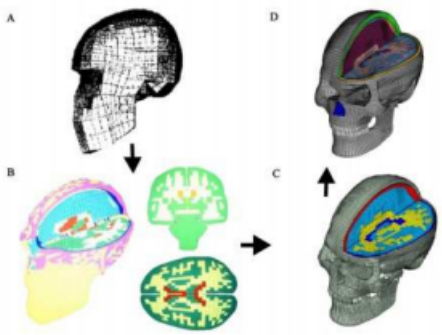

Figure 2.11: Different iterations of the WSUBIM FEHM - Retrieved from [8]

Another FEHM that is worth remembering is the Louis Pasteur developed by Kang and Willinger in 1997 [55]. This model used isotropic and homogeneous material properties for the CSF, tentorium, skull and scalp and falx while for the brain the material model used was the viscoelastic. The novelty of this model was the introduction of a Lagrangian approach to model the CSF and an elastic-brittle constitutive law for the skull-brain interface [8].

This model weighs 4,8 Kg, consists of 13208 brick elements and 2813 shell elements and makes it possible to calculate internal brain pressure as well as validate longer tests over 15 ms.

In table 2.8 we can analyse the tolerance limits for different types of traumatic brain injuries established by this model and in table 2.9 a resume of the prominent FEHM's found in literature, their development year, and the validation method adopted.

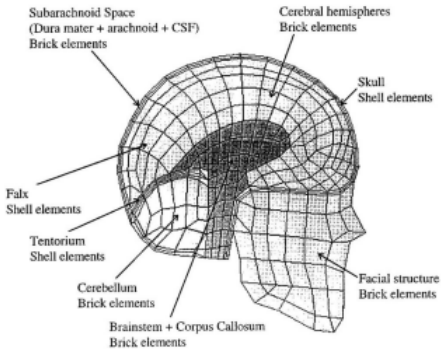

Figure 2.12: University of Louis Pasteus FEHM - Retrieved from [51]

Table 2.8: Head injury limits for the Louis Pasteur FEHM - Adapted from [7]

Calculated mechanical parameter and injury indicator	**Injuries**	**Uninjured**	**Possibly injured**	**Injured**
Brain pressure [kPa]	Brain contussion	160	160 240	340
Brain von Mises stress [kPa]	Brain moderate neurological injuries	14	14 22	22
Brain von Mises stress [kPa]	Brain severe neurological injuries	30	30 46	46
Global strain energy of the brain-skull interface [mJ]	Subdural or subarachnoid haematoma	4300	4300 6500	6500
Global strain energy of the skull [mJ]	Skull fracture	1700	1700 2700	2700

Table 2.9: Resume of prominent FEHM's found in literature - Adapted from [8]

Authors	**Year**	**Dimension**	**Model descriptions**	**Validation**
Hardy and Marcal [12]	1971	2D	Liner elastic skull	
Kenner and Goldsmith [13]	1972	3D	Compressible, inviscid fluid in axisymmetrical, thin, spherical shell (elastic for the skull shell; viscoelastic for the brain fluid)	
Nickell and Marcal [56]	1974	2D	Linear elastic skull for vibration response study	
Chan [57]	1974	3D	Modelled the human head as a linearly viscoelastic core bonded to a linearly viscoelastic spherical shell and a prolate ellipsoid.	
Shugar [58]	1975	2D	3-layered fluid-filled skull with brain modelled as homogeneous, nearly incompressible fluid	
Shugar and Kahona [59]	1977	3D	Thin layer modelled as subarachnoid space between the skull and the brain.	
Ward and Thompson [60]	1975	3D	Rigid skull shell with linearly elastic core and CSF	

Table 2.9 continued from previous page

Authors	Year	Dimension	Model descriptions	Validation
Khalil and Hubbard [61]	1977	2D	Fluid-filled, single-layered or mulit-layered circular and ellipsoidal shells (elastic for the scalp and the skull layers; viscoelastic for the brain fluid)	
Nahum [10]	1977	3D	Linear elastic solid brain.	Pressure
Hosey and Liu [62]	1981	3D	Homomorphic head and neck model including scalp, skull, falx, dura, CSF, brain and spinal cord and cervical column.	Initial inertia characteristics of the brain
Ueno [63]	1989	2D	2D model by including layered rigid skull and linear elastic brain. Advanced 2D model by including layered rigid skull and linear elastic brain	Pressure
	1991	2D		
Ruan [32]	1993	3D	Developed the Wayne State University Brain injury model (WSUBIM) version I, which included the scalp, the 3 layered skull, CSF, dura matter, falx cerebri and brain.	Pressure
	1994	3D		

Table 2.9 continued from previous page

Authors	Year	Dimension	Model descriptions	Validation
Zhou [33]	1995	3D	Improved on WSUBIM version I by using finer elements Pressure; Relative motion magnitude	
Kang and Willinger [55]	1997	3D	Developed by the University of Louis Pasteur, Strasbourg; Finite Element Head Model (ULP FEHM)	Stress
	1999	3D		Pressure
Kumaresan and Radhakrishna [64]	1996	3D	Homeomorphic head and neck model which consisted of the skull, CSF, the brain, its partitioning membranes (falx cerebri and tentorium cerebelli) and the neck.	
Zhang [54]	2001	3D	Improved and constructed WSUBIM version II by improving the facial features and introducing a sliding interface between linearly elastic skull and viscoelastic brain.	Pressure

Table 2.9 continued from previous page

Authors	Year	Dimension	Model descriptions	Validation
King [39]	2003	3D	Latest and completely revised WSUBIM with viscoelastic brain, elastic-plastic bones.	
Kleiven and Hardy [65]	2002	3D	Developed the Kungliga Tekniska Hogskolan (Royal Institute of technology) Finite Element Head Model (KTH FEHM) which consists of the scalp, skull, brain, meninges, CSF, 11 pairs of parasagittal bridging veins and a simplified neck and included sliding condition between skull and brain	Pressure and Relative motion
Horgan and Gilchrist [36]	2003	3D	Developed the University College Dublin Brain Trauma Model (UCDBTM) which includes a scalp, a 3 layered skull, dura, CSF, Pia.	

2.5.1 Material models of the different FEHM

The materials used in FE simulation are of great importance since it defines the response behaviour of the model when external loads are being applied. Hence a literature review of the material models used by important FEHM was conducted and the summary is presented in the table below.

Table 2.10: Material models and properties used by different FEHM - Adapted from [8]

Components	**Material Properties**				
	Model Type	**Young's Modulus, E (MPa)**	**Poisson's ratio, ν**	**Density, (kg/mm3)**	**Bulk Modulus/ Compressibility, K (MPa)**
Brain (as a whole)	Linear Elastic	8,00E-02	0,49		
	Linear Elastic	6,67E-02	0,48		
	Linear Elastic	6,75E-01		1,14E-06	5,63E+00
	Linear Elastic			1,03E-06	2,19E+03
	Linear Elastic		0,4996	1,04E-06	2,19E+03
	Hyperelastic				
	Hyperelastic		0,499981	1,04E-06	
CSF	Linear Elastic		0,45	1,13E-06	1,10E-04
	Linear Elastic	2,19E+00	0,489	1,04E-06	
	Linear Elastic		0,5	1,00E-06	2,10E+03
	Linear Elastic		0,5	1,00E-06	2,19E+03
	Linear Elastic	1,00E-05	0,499		
	Linear Elastic	1,20E-02	0,49		
Dura Mater	Linear Elastic	3,15E+01	0,45	1,13E-06	
	Linear Elastic	3,15E+01	0,45	1,14E-06	
Falx	Linear Elastic	3,15E+01	0,23	1,14E-06	
	Linear Elastic	3,15E+01	0,45	1,13E-06	
	Linear Elastic	3,15E+01	0,45	1,14E-06	
Foramen	Linear Elastic	6,93E+03	0,45	1,05E-06	
Pia mater	Linear elastic	1,15E+01	0,45	1,13E-06	

2.5.2 Boundary conditions

Boundary conditions (BC) are assigned to a FEHM and define how the different parts of the geometry interact with each-other hence it has a critical role in defining the mechanical response of the model. The BCs assigned to a model are not yet clearly defined in the literature and depend heavily on the model itself, however the Skull-Brain interface has been highlighted by several researchers [8].

In the table presented below a summary of the BCs applied to different head models is presented.

Table 2.11: Literature review of BCs applied to several FEHM - Adapted from [8]

Authors	**Year**	**Dimension**	**CSF**	**Skull-Brain interface**	**Foramen magnum**
Shugar and Kahona [60]	1975	3D	Linear elastic solid elements	Common nodes	Not modeled
Ueno [63]	1989	2D	Linear elastic solid elements	Tied nodes	Free nodes

Table 2.11 continued from previous page

Authors	Year	Dimension	CSF	Skull-Brain interface	Foramen magnum
DisMasi [66]	1991	3D	Linear elastic solid elements	Combination of sliding and fixed	Not modeled
Ruan [32]	1994	3D	Linear elastic solid elements	CSF modeled as a solid element	Upper brainstem modeled
Zhou [33]	1995	3D	Linear elastic solid elements	Combination of tied nodes and sliding w/o separation	Upper brainstem is modeled
Kumaresan and Radhakrishnan [64]	1996	3D	Linear elastic solid elements	CSF modeled as a solid element	No information
Killinger and Kang [35]	1999	3D	Linear elastic solid elements	CSF modeled as a solid element	Not modeled
Zhang [54; 67]	2001	3D	Linear elastic solid elements	Sliding w/o separation	Upper brainstem is modeled
	2001	3D	Linear elastic solid elements	Tied interface	Upper brainstem is modeled
	2002	3D	Linear elastic solid elements	Tied interface between skull and dura; sliding interface between meninges and brain	Brainstem is modeled
Kleivein and hardy [65; 68]	2003	3D	Linear elastic solid elements	Tied interface between skull and dura; sliding interface between meninges and brain	Brainstem is modeled
	2006	3D	Linear elastic solid elements	Tie-break interface	Not modeled
Takhounts and Eppinger [69; 70]	2008	3D	Linear elastic solid elements	Tied interface (due to numerical difficulties)	Upper brainstem is modeled

2.5.3 YEt Another Head Model (YEAHM)

The YEAHM is a finite element head model developed by Fernandes and further improved by students of the University of Aveiro. Although there are several different head models developed this one differs from the others because it takes into account the influence of sulci and gyri which is not considered by other head models. This is an important factor since it plays a considerable effect in von Mises maximum stress.

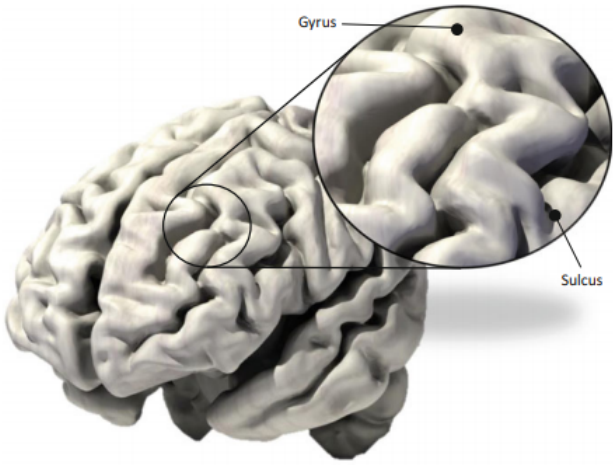

Figure 2.13: Sulci and gyri present in [9] FEHM - Retrieved from [9]

The YEAHM head model includes the skull, brain, CSF, superior sagitall sinus and respective bridging veins.

The brain geometry includes all the important sections: frontal, parietal, temporal, occipital, both hemispheres, cerebrum, cerebellum, corpus callossum, thalamus, midbrain and brain stem.

In this head model, all the elements with the exception of superior sagittal sinus and the bridging veins were modelled as a solid due to their complex geometry and meshed with tetrahedral elements.

Geometric modelling

As per the author [9] this head model was developed through medical images, more specifically computer tomography (CT) and magnetic resonance imaging (MRI). The CT was used to model bone structures while MRI was more applicable to extract information about soft tissues like the cerebrum. After achieving a primary head model through segmentation of medical images the model was further detailed using Meshmixer to smooth out some imperfections and Meshlab to close geometry gaps. After finishing the geometric model it was then imported to CATIA software so a 3D solid could be generated and the space between the skull and brain was used to model CSF.

Material modelling

For the brain tissue, this model uses a hyper-viscoelastic model to describe it and the properties used can be seen in table 2.12

Table 2.12: Brain modelling properties - Retrieved from [9]

ρ $[Kg/m^3]$	μ [MPa]	α_1	D1 $[Mpa^{-1}]$	g_1	g_2	τ_1 [s]	τ_2 [s]
1040	0,012	5,0507	0,04	0,5837	0,2387	0,02571	0,02570

The CSF was modelled as a solid with low shear modulus using Mooney-Rivlin strain energy potential hyperelastic model also the relation $C_{10} = 0,9 \times C_{01}$ was adopted. The properties used are shown in 2.13.

Table 2.13: Properties used to model the CSF - Retrieved from [9]

ρ $[Kg/m^3]$	C_{10} [MPa]	C_{01} [MPa]	D_1 $[Mpa^{-1}]$
1000	0,9	1	0,9

The first skull bone geometry was modelled using a single isotropic linear elastic material and the properties used are presented in the table 2.14 presented below.

Table 2.14: Skull material modelling properties - Retrieved from [9]

ρ $[Kg/m^3]$	E [MPa]	ν
1800	6000	0,21

Yet this geometry was further developed by Barbosa [71] and now include material differentiation between the different bones that constitute the skull namely: trabecular and cortical but also for the sutures. The properties for the new skull are shown in the table 2.15

Table 2.15: material model properties for the new skull geometry

Geometry	Young modulus [Mpa]	Density [kg/m3]	Poisson
Trabecular	1000	1500	0,05
Cortical	20000	1900	0,21
Sutures	1500	1500	0,3

Boundary conditions

The boundary conditions applied to the model were in terms of the relative motion between the brain and skull. This was defined using a sliding interface between the skull and the CSF and between the CSF and the brain using for the effect a kinematic contact method with a friction coefficient for tangential behaviour of 0,2 [9].

.

Chapter 3

Methodology

In this chapter the implementation of the method as well as all the software, materials models and methods used in the elaboration of this work are presented.

3.1 Fluid cavity method

The fluid cavity modelling technique arises from the need to understand the response of a fluid-filled or gas-filled structure.This method works best when the response of the structure depends on external loads but also on the pressure exerted by the fluid; this effect is achieved by using hydrostatic fluid elements that provide the coupling needed. To prescribe this method it is needed a surface defining the boundary of the fluid cavity, which in this work will be the surface anatomically representing the dura mater and a cavity reference point.

Given its properties, this technique of discretizing fluid filled structures could be applied to model CSF assuming CSF as being a confined fluid and solve the problem of mesh distortion of the current technique used to model CSF. Hence this method will be tested. The methods and properties used to apply this technique will be discussed in this chapter.

3.1.1 Discretizing the fluid cavity

The hydrostatic fluid elements are surface elements that cover the boundary of the fluid cavity. In places where standard finite elements are used to model the boundary of the cavity, the hydrostatic fluid elements share the nodes at the cavity boundary with the standard elements as can be seen in figure 3.1.

These elements must be associated with a common node referred to as the cavity reference node. In cases where the boundary of the fluid filled cavity is symmetric and thus only a part is modelled the reference node must lie in the symmetry plane whereas in a non symmetric boundary the condition is that the node should lie within the cavity .

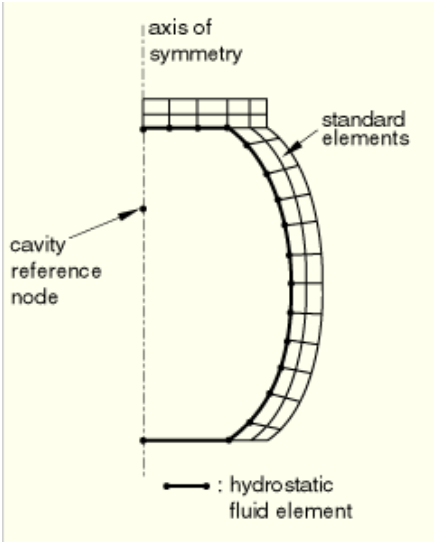

Figure 3.1: Hydrostatic fluid elements - Retrieved from [72]

3.1.2 Dura mater geometry

As stated before prescribing the fluid cavity method requires defining the boundary (surface) that bounds the fluid cavity. Anatomically this surface is materialised by the dura mater (the outer boundary layer of the CSF) which is in contact with the skull.

The geometrical model of the dura mater started with a change in the assembly geometry positions since the last version the assembly contained parts that were too close for the boolean function to be able to work and therefore this problem had to be resolved. To address this issue the brain was moved a millimeter to the left since the interceptions were located in the right hemisphere and the interceptions were resolved.

After this step was concluded the YEAHM model containing the skull and the brain was exported as an STL file from Abaqus to MeshMixer that is a "state of the art" open source software that enables manipulation and edition of triangular meshes.

Subsequently a cube geometry bigger than the model was imported into the assembly and a boolean operation between the parts was performed resulting in a primary geometry for the dura mater. Since the skull is perforated in the neck area (image 3.3) the geometry also presented a hole that posteriorly had to be resolved.

After the primary model was obtained it was necessary to do further alterations to the geometry so the method of fluid cavity in Abaqus could be executed. These alterations concerned making the new CSF geometry an enclosed surface and also not intercept the geometries already included in the model since it would produce errors in Abaqus solver.

The interception was between the the new dura matter geometry and the medulla region of the brain. To solve this problem the "*inflate*" function was used in meshmixer, so the dura mater geometry was "pulled down" creating a space between the medulla zone of the brain and the new dura mater geometry resolving the interception. After inflating operation, the geometry presented some "bumps" which were reduced by using the

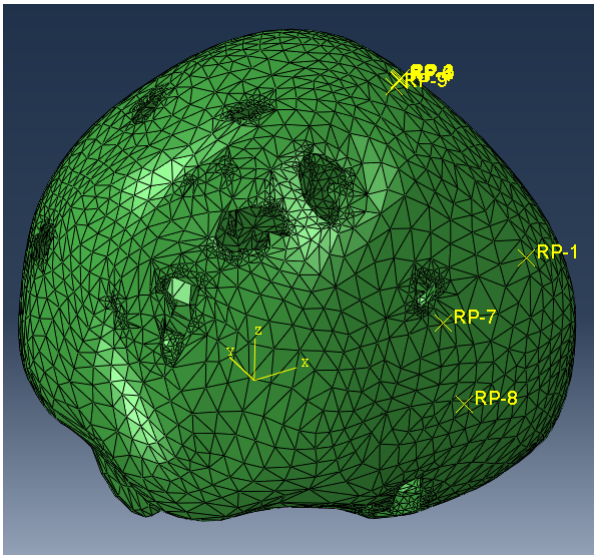

Figure 3.2: Original cerebrospinal fluid geometry.

"*RobustSmooth*" tool in the same software creating a smoother geometry.

Besides the operation previously described, in the same software, the inspector tool was also used. This function performs an analysis on the geometry advising the designer whether the geometry has small holes and other problems to be resolved. The geometry with the holes problem resolved is shown in 3.4 and the inflation detail in figure 3.5

The geometry obtained was subsequently meshed in "hypermesh" which is a software that possesses geometry and meshing capabilities.

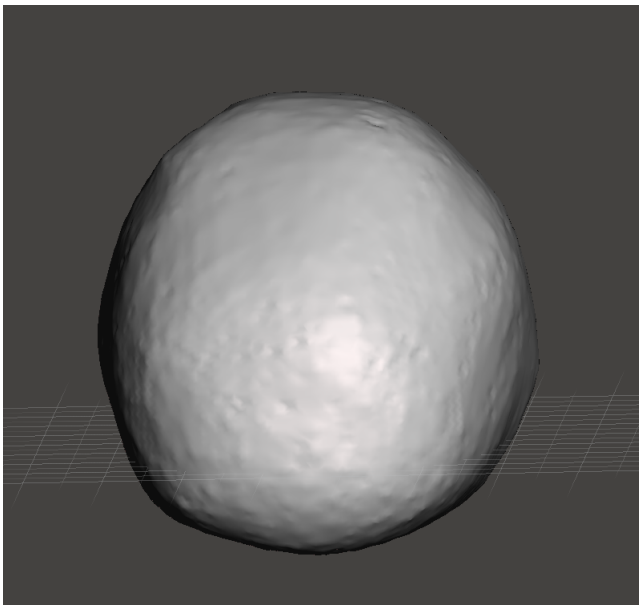

Figure 3.4: New dura matter geometry - front view.

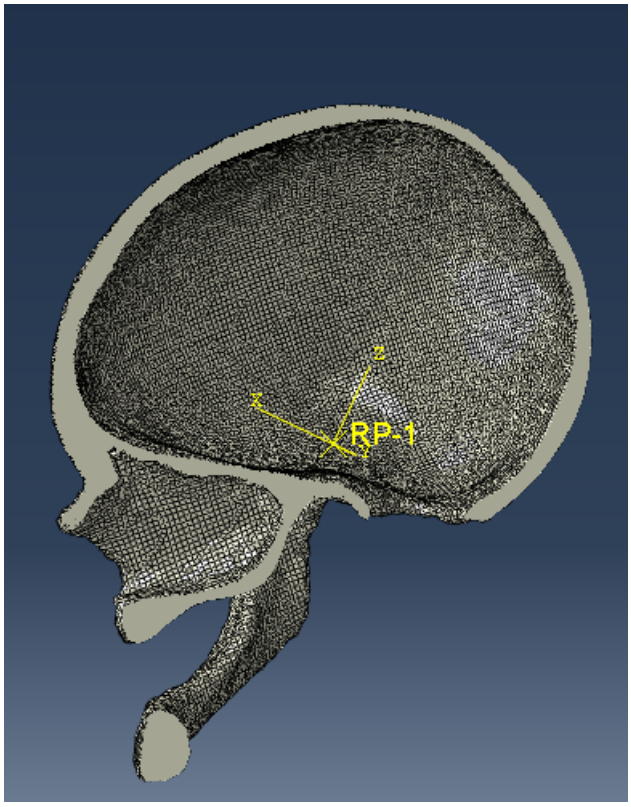

Figure 3.3: Illustration of the cranium orifice.

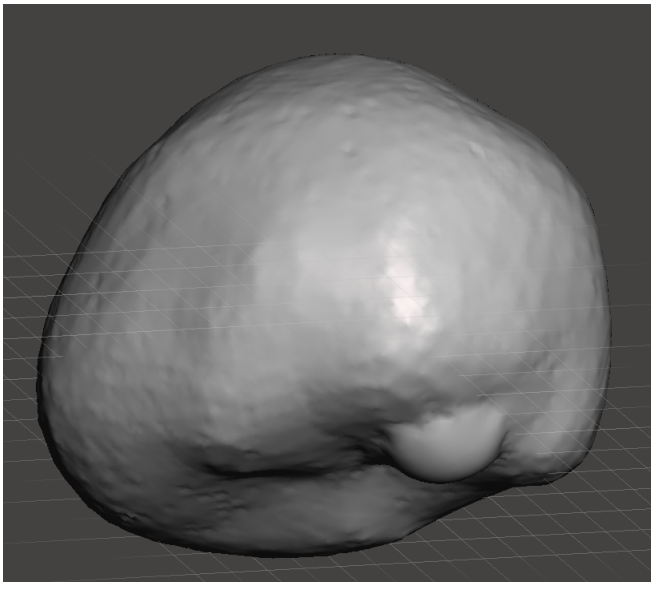

Figure 3.5: New dura matter geometry - Inflation detail.

3.1.3 Material models used

Dura mater material model

In the studies reviewed the dura matter material model and property values was well established across a variety of different authors varying residually in terms of density. Hence the material model used was of type linear elastic and the property values can be seen in the table 3.1 below.

Table 3.1: Parameters used to define the Dura mater material model

Parameter	**Value**	**Unit**
Young modulus (E)	31.5	MPa
Poisson ratio (ν)	0.45	
Density ρ	1.45×10^{-9}	Ton/mm^3

CSF material model

In the fluid cavity method there are two possible models to define the fluid: the hydraulic and the pneumatic. Since the cerebrospinal fluid is a liquid the method used was the hydraulic.

The compressibility of the fluid in this method is introduced by assuming a linear relationship between pressure and volume and the required input parameter to do so are the reference density and the bulk modulus. The compressibility is then described by the bulk modulus through the following equation:

$p = -K\left(\frac{V(p,\theta)-V_0(\theta)}{V_0(\theta_I)}\right) = -K\rho_R(\rho^{-1}(p,\theta) - \rho_0^{-1}(\theta))$

where:

- p - is the current pressure.
- θ - is the current temperature.
- K is the bulk modulus.
- $V(p,\theta)$ is the current fluid volume.
- $\rho(p,\theta)$ is the density at current pressure and temperature.
- $V_0(\theta)$ is the fluid volume at zero pressure and current temperature.
- $V_0(\theta_I)$ is the fluid volume at zero pressure and initial temperature.
- $\rho_0(\theta)$ is the density at zero pressure and current temperature.

Bulk modulus is defined as a measure of how resistant to compression a given substance is. More specifically the bulk modulus is defined as the ratio of infinitesimal pressure increase to the resulting relative decrease in volume.

By default Abaqus assumes the bulk modulus to be independent from the change in fluid density. Cerebrospinal fluid is mainly composed of water (99%) hence water properties were used when defining the bulk modulus and density which were in accordance with the

values reported by the literature. The properties values used to define the cerebrospinal fluid are presented in the table below.

Table 3.2: Parameters used to define the Cerebrospinal fluid

Parameter	**Value**	**Unit**
Bulk modulus	2100	MPa
Density	9.96×10^{-10}	Ton/mm^3

3.1.4 Boundary conditions applied

In this case the boundary conditions applied to the model relate to the tests performed by Nahum [10]. In this case the head of the cadaver was restrained by a metallic frame that inhibited the lateral movement but not the anterior posterior movement. Having this and the fact that the projectile only has a translational in terms of movement no boundary conditions were necessary to perform the simulation since the force caused by the impactor didn't produce any rotation velocity that had to be suppressed.

Yet in the experiments used for validation the cadaver head was pressurised to in-vivo levels therefore a predefined field of cavity pressure was applied to the fluid cavity interaction with the value of $0,02399803$ MPa [73].

3.2 Validation methodology

The validation model of this new geometry and method will be based on Nahum experiments [10], to be more precise the number 37 since its the most commonly used to validate proeminent FEHM. This method of validation focus on the intracranial pressure response of the human head.

In Nahum experiments the human head suffers a blunt impact in the frontal area, the head is rotated 45°from the Frankfurt plane so the projectile hits the head perpendicularly as can be seen in image below.

In the same experiments Nahum tests a number of different impact objects, materials, masses, velocities and then records the pressure response in the different parts of the human head namely: frontal, parietal, two occipital zones (1 and 2), posterior fossa and also in the carotid siphon.

The author is not precise in which materials were used in the impactor nor on the exact locations where the pressure values were acquired, only referring to the zones in broad terms. To resolve the first issue the input curve force supplied will be used to check whether the implementation of the method is precise, the second issue is solved by performing an average of the pressure values for several elements that are located at the zones referred in the study.

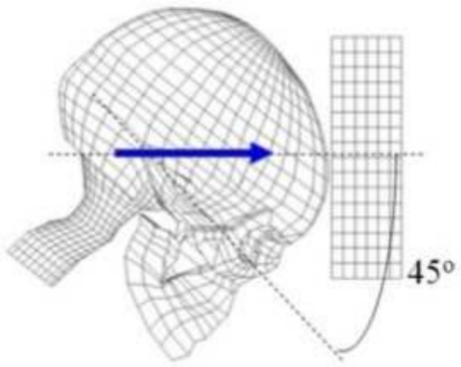

Figure 3.6: Illustration of the simulation performed by [10] - Retrieved from [8]

Impactor Properties					Pressures (kPa)					
Experiment #	Mass (kg)	Velocity (m/s)	Impact Force (kN)	Acceleration ($\times 10^3$ m/s^2)	Frontal	Parietal	Occipital 1	Occipital 2	Posterior Fossa	Carotid Siphon
Series 1										
36	5.36	8.75	7.78	2.30	136	79	−27	−10	−64	–
37	5.59	9.94	7.90	2.00	141	74	−45	−48	−60	–
38	5.32	9.60	10.80	2.42	139	66	−27	–	−65	–
41	23.09	12.83	14.84	2.42	428	189	114	–	−57	47
42	5.23	12.95	5.20	3.90	–	9	–	–	−44	73
43	5.23	12.95	10.59	2.23	271	222	64	–	−18	108
44	5.23	4.36	6.53	1.52	102	20	15	–	−2	115
54	5.23	8.41	10.84	2.34	275	181	33	–	−64	48
Series 2										
46	5.23	4.42	1.50	0.31	–	–	–	–	–	–
47	5.23	4.42	1.22	0.29	–	–	–	–	–	–
48	5.23	4.21	4.27	1.28	–	–	–	–	–	–
49	5.23	8.35	9.35	3.42	–	–	–	–	–	–
50	5.23	8.35	6.28	1.49	–	–	–	–	–	–
51	5.23	8.29	16.60	5.39	–	–	–	–	–	–
52	5.23	8.69	13.34	4.29	–	–	–	–	–	–

Table 3.3: Nahum [10] impact peak values retrieved from the various experiments performed

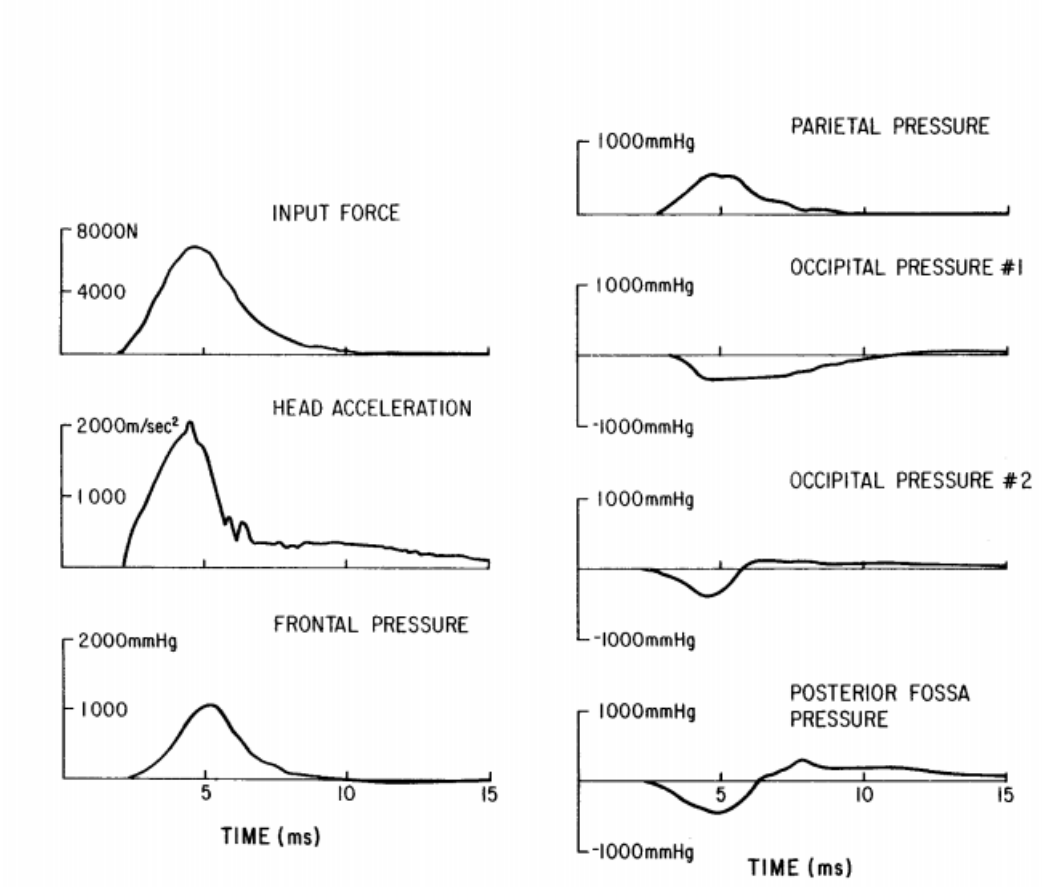

Figure 3.7: Nahum impact values retrieved from the 37 experiment [10]

Chapter 4

Simulation and results

The simulations presented in the following chapter were carried out using a dynamic explicit analysis performed in Abaqus software.

This type of analysis is a computationally efficient method to deal with large models with a short dynamic response time and for the analysis of extreme discontinuous processes; it also has advantages such as: the use of small increments which allows the solution to proceed without iterations and no requirement of calculating tangent stiffness matrices and the simplification of contact [74].

In the simulations performed the interaction between parts was considered as a general contact with penalty contact type with a friction coefficient of 0.2.

A cylindrical impactor with a volume of 22620 mm^3 was modelled to recreate the impact. This impactor used an elastic material model with the properties shown on table 4.1 it was then prescribed a predefined field of velocity of 6630 mm/s which is not the value actually reported from literature but was the velocity that resulted in the best depiction of the input force reported by [10]. Since the material of the various pads utilised in the real experiments is not well described in the experiments the previous logic of using the material models that best depict the input force curve was followed.

Table 4.1: Parameters used to define the impactor material model

Parameter	**Value**	**Unit**
Young modulus	6	Mpa
Density	1.4×10^{-9}	Ton/mm^3
Poisson	0.16	–

To test this method the assembly with skull, dura matter and the brain was considered although the original model contains a superior sagittal sinus and bridging veins geometry. The reason for this is that the model has a tight tolerance between different components and it was not possible to add the needed dura matter geometry without changing those geometries.

At first the reported values for the bulk modulus as depicted in chapter 3 were used in the simulations yet those produced pressure values which were order of magnitude above literature values therefore this value had to be adjusted via trial and error to 2.1 Pa which although it is several orders of magnitude below those reported on the literature for CSF worked best in our case.

The initial overclosures with the skull that derive from the discretization of the geometry were resolved using the "*strain free adjustment*" option that as the name implies doesn't produce strain while adjusting nodes that may intersect.

In order to enable a comparison with the experimental results obtained in Nahum [10] experiments the graphs presented in figure 3.7 were imported to graphreader application [75] where the acquisition of the pressure curves for the different regions and for the impact force took place.

The meshes utilised throughout the simulation described above can be seen in the figures below. In figure 4.1 we can see S3 element mesh utilised, in figure 4.2 the S4 coarse mesh and in figure 4.3 the refined S4 element mesh.

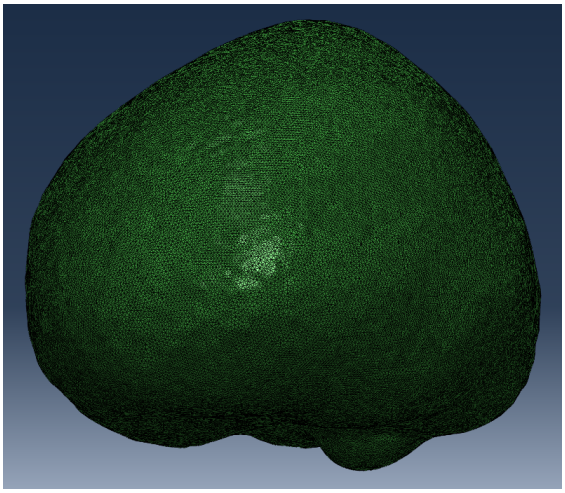

Figure 4.1: Triangular S3 element - mesh utilised

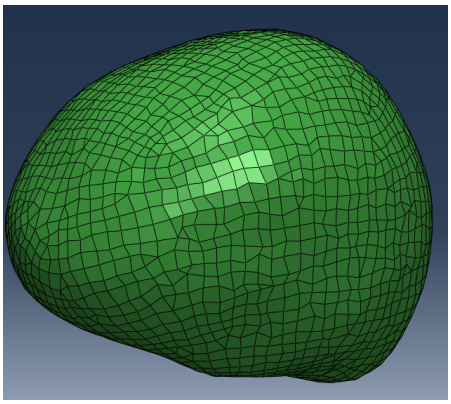

Figure 4.2: Quadrangular S4 element - mesh utilised

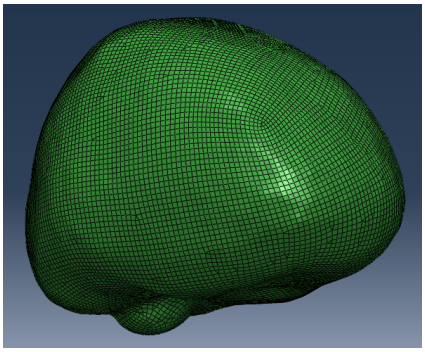

Figure 4.3: Quadrangular S4 element - refined mesh utilised

4.1 Simulation validation

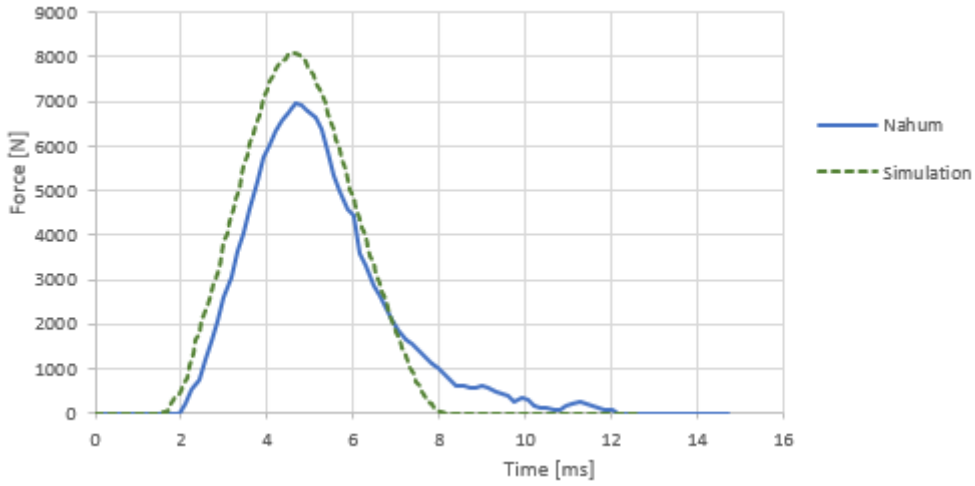

Figure 4.4: Input force comparison

The input force at the point of impact was measured in order to assess the validity of the test. As can be observed in figure 4.4 the input force obtained is a bit larger than the actual curve reported by Nahum [10] in yet when we examine in detail image 4.2 of the peak pressures a difference between the peak value on the curve and those on the table for the 37^{th} experiment differ in about 1000 N therefore the peak value of 7900 N is used and the curve obtained in this study is considered valid.

Table III - Series I

Experiment	Peak Input Force ($N \times 10^3$)	Peak Head Acceleration ($m/s^2 \times 10^3$)	Pressures: Frontal (mm Hg)	Parietal	Occipital #1	Occipital #2	Posterior Fossa	Carotid Siphon (mm Hg)
36	7.78	2.30	1022	594	-205	-78*	-480	-
37	7.90	2.00	1059	552	-341	-363	-452	-
38	10.80	2.42	1041	494	-205	-	-485	-
41	14.84	3.90	3207	1414	857	-	-426	352
42	5.20	1.59	-	70	-	-	-329	550
43	10.59	2.23	2031	1664	482	-	-136	811
44	6.53	1.52	764	150	109	-	- 19	860
54	10.84	2.34	2059	1354	248	-	-483	356

* epidural

Table 4.2: Peak pressure values - Retrieved from [10]

4.2 Results

The dura matter geometry was first meshed using S3 elements and contained 173 862 elements and 86 843 nodes. This mesh had overall a high quality since no elements were found with a jacobian value inferior to 0.6, the average aspect ratio of elements of this mesh is 1,17.

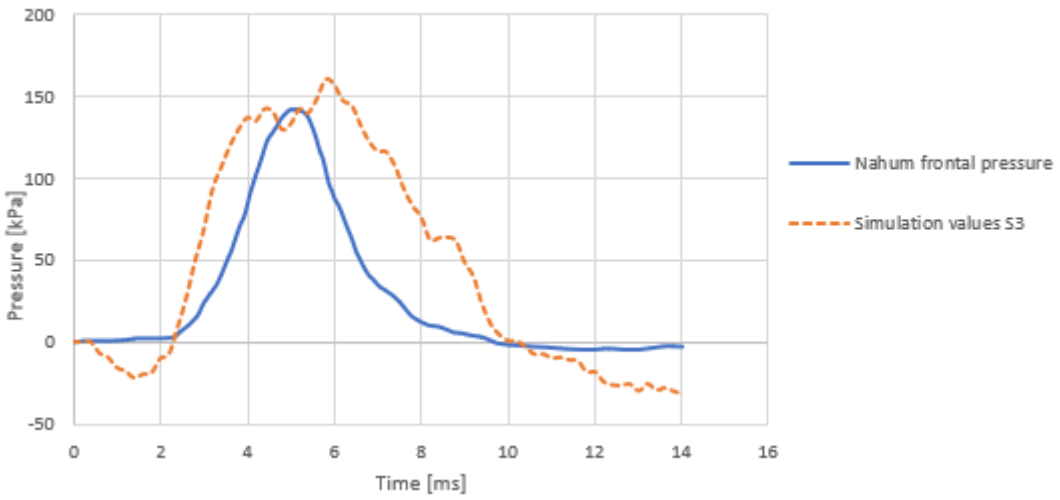

Figure 4.5: Frontal pressure comparison - S3 element

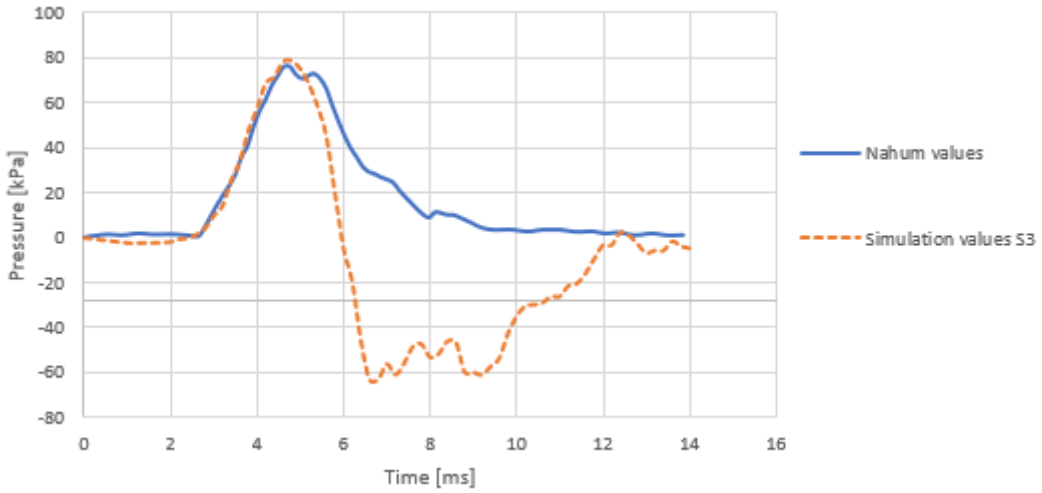

Figure 4.6: Parietal pressure comparison - S3 element

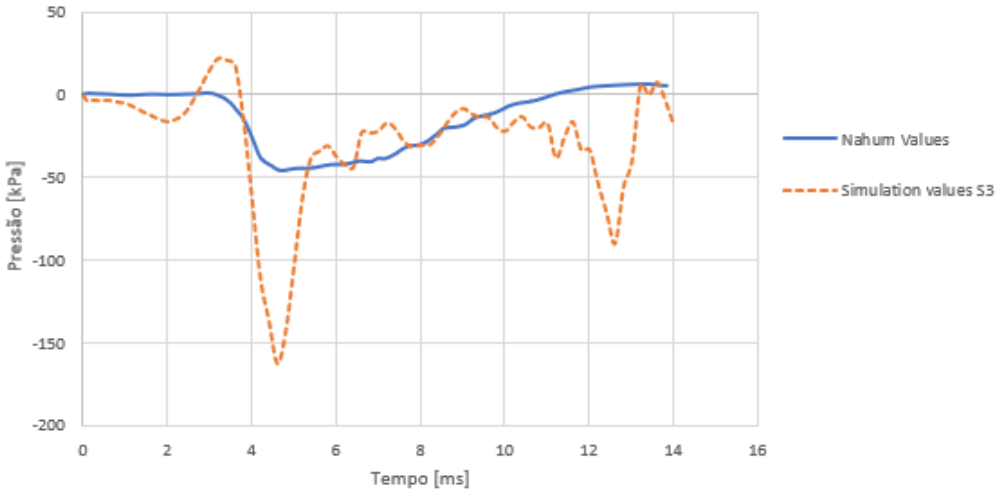

Figure 4.7: Occipital 1 pressure comparison - S3 element

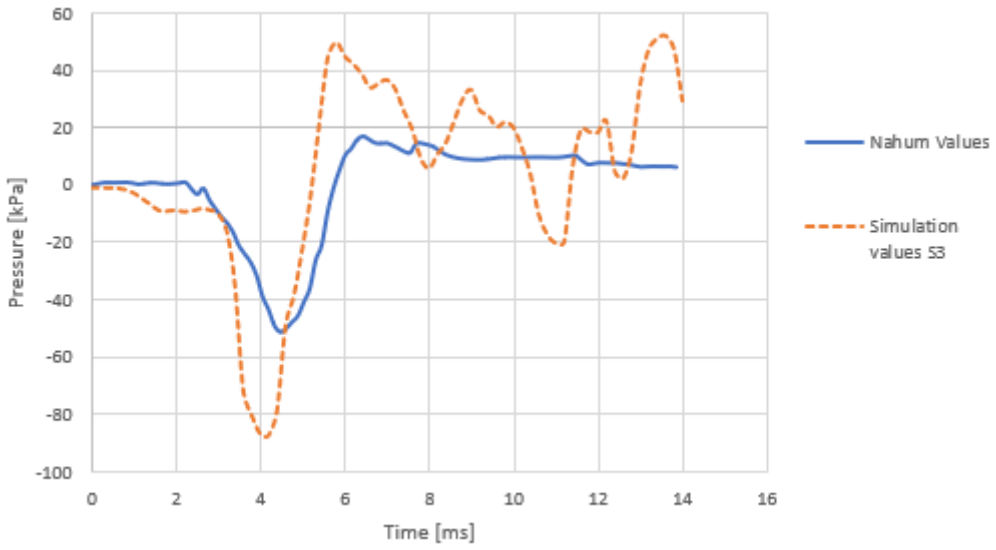

Figure 4.8: Occipital 2 pressure comparison - S3 element

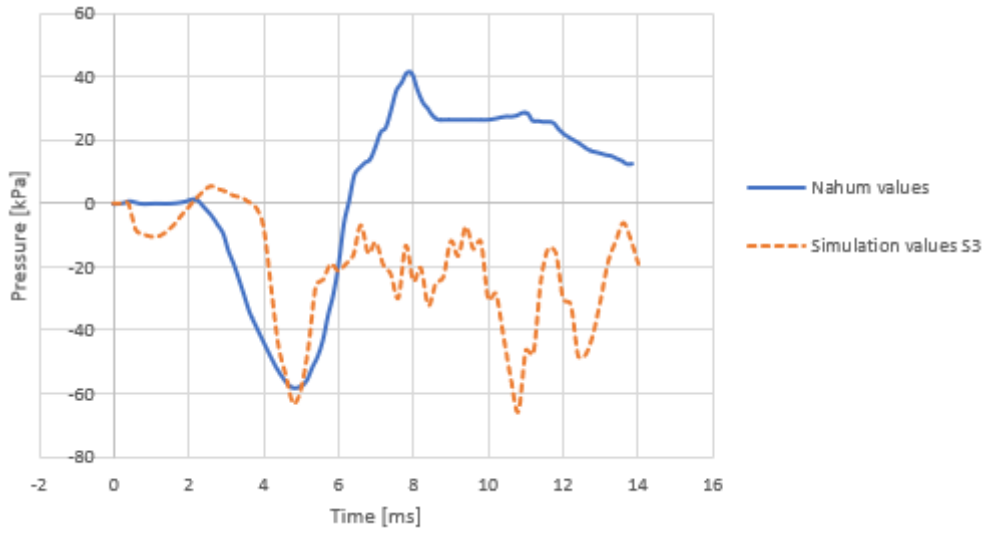

Figure 4.9: Posterior fossa pressure comparison - S3 element

As can be observed from the graphs the values obtained from this method with the S3 element type didn't produce accurate results when compared to the ones already obtained by Fernandes [9], therefore the S4 element was tested with the aim to improve results since it had worked well for [53].

The change for the S4 element type introduced more nodes and the level of refinement of the S3 mesh was found excessive therefore the mesh was reduced in order to maintain the simulation computationally efficient. The new mesh contained 2989 elements and 2888 nodes. This mesh as the previous had good overall quality with all the elements with a jacobian value above 0,6, only 1,1 % of elements with a skew value above 0,5 and

an average aspect ratio of 1.51.

This mesh also didn't result in more accurate results than those already obtained so the reduced version of the S4 element, the S4R, with the same mesh density was tested.

The results for this mesh can be seen in the figures below and a comparison between the S4 and S4R element is drawn. From the graphs analysis it can be observed that both elements improved the accuracy of the results in certain areas such as the parietal, occipital 1 and posterior fossa but not in all when compared with the S3 element with the S4R showing the best results.

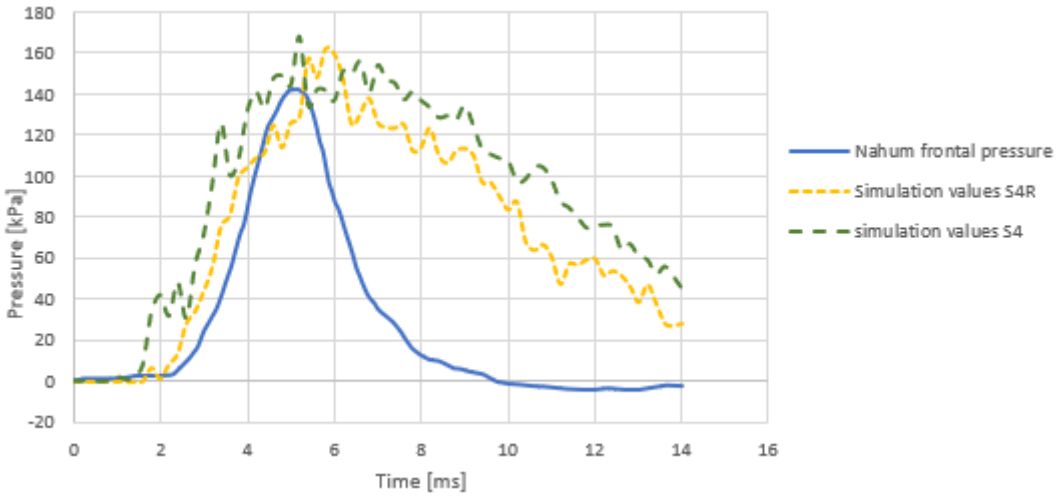

Figure 4.10: Frontal pressure comparison - S4 and S4R elements

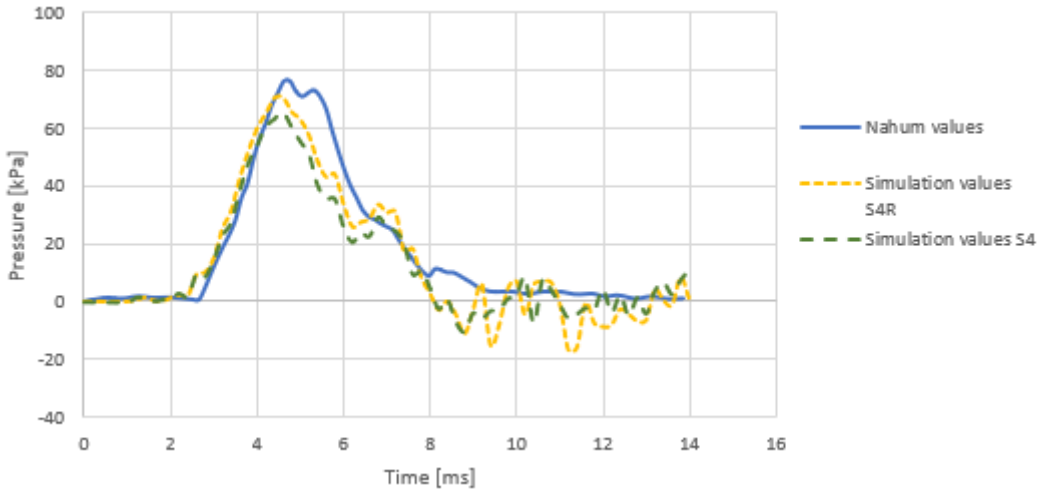

Figure 4.11: Parietal pressure comparison - S4 and S4R elements

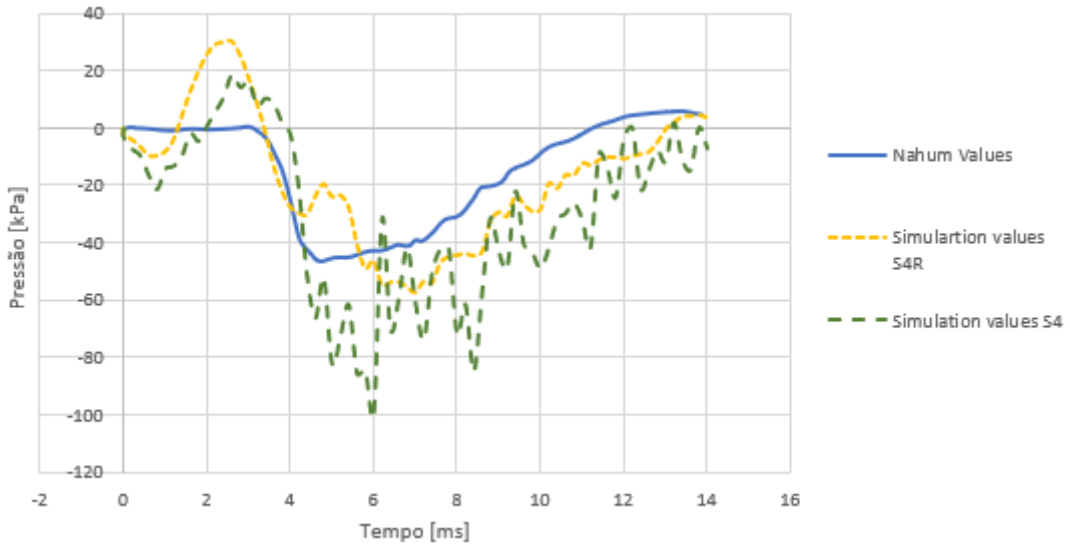

Figure 4.12: Occipital 1 pressure comparison - S4 and S4R elements

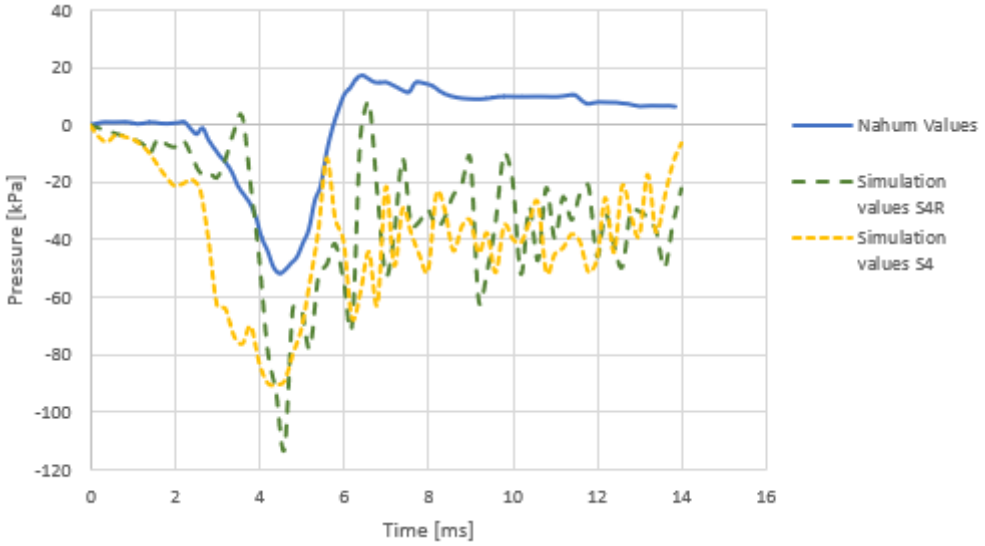

Figure 4.13: Occipital 2 pressure comparison - S4 and S4R elements

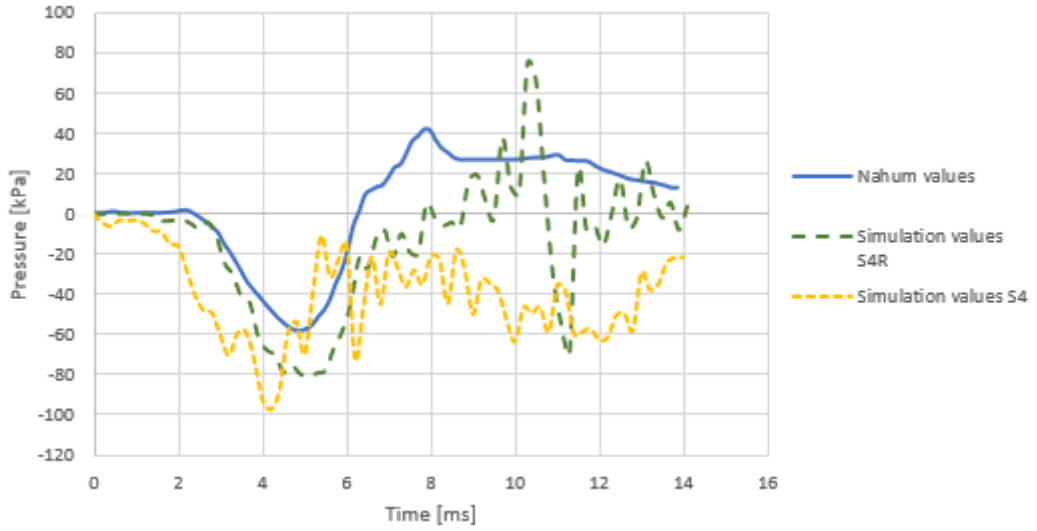

Figure 4.14: Posterior fossa pressure comparison - S4 and S4R elements

Since the mesh reduction was abrupt going from 173 862 elements to a 2989 elements we tried refining the S4R mesh since it seemed to be the one that had the best overall results. The refined mesh ended up having 17 284 elements and 17 074. The S4R refined mesh had an average aspect ratio of 1,25, and no elements with a skewness above 0,5.

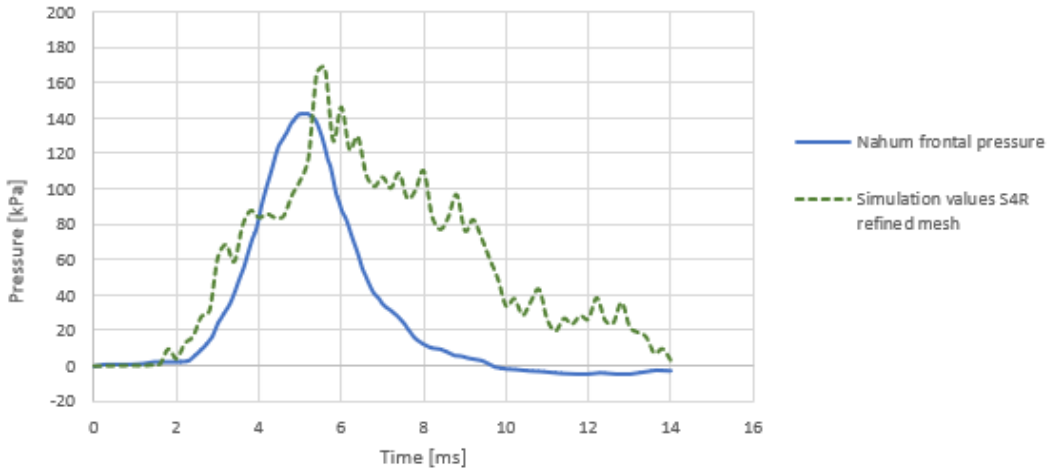

Figure 4.15: Frontal pressure comparison - S4R element with refined mesh

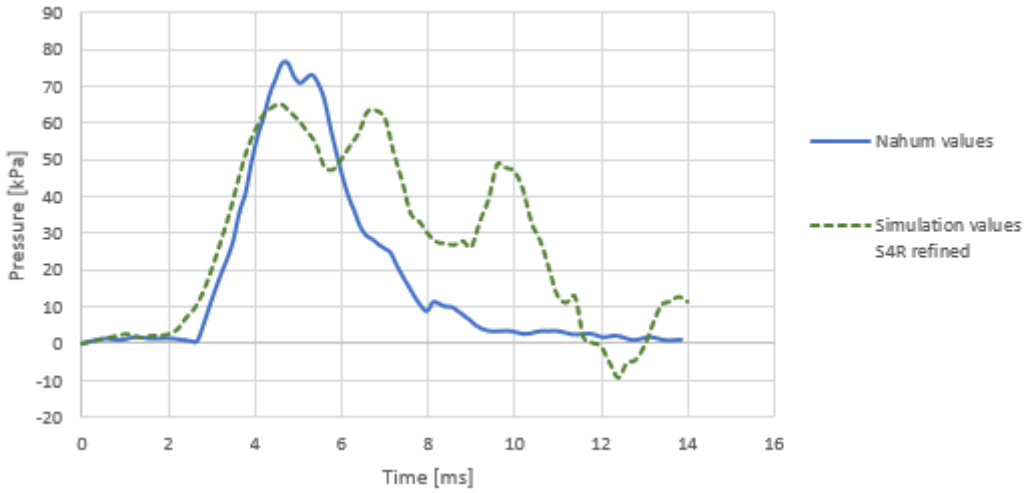

Figure 4.16: Parietal pressure comparison - S4R element with refined mesh

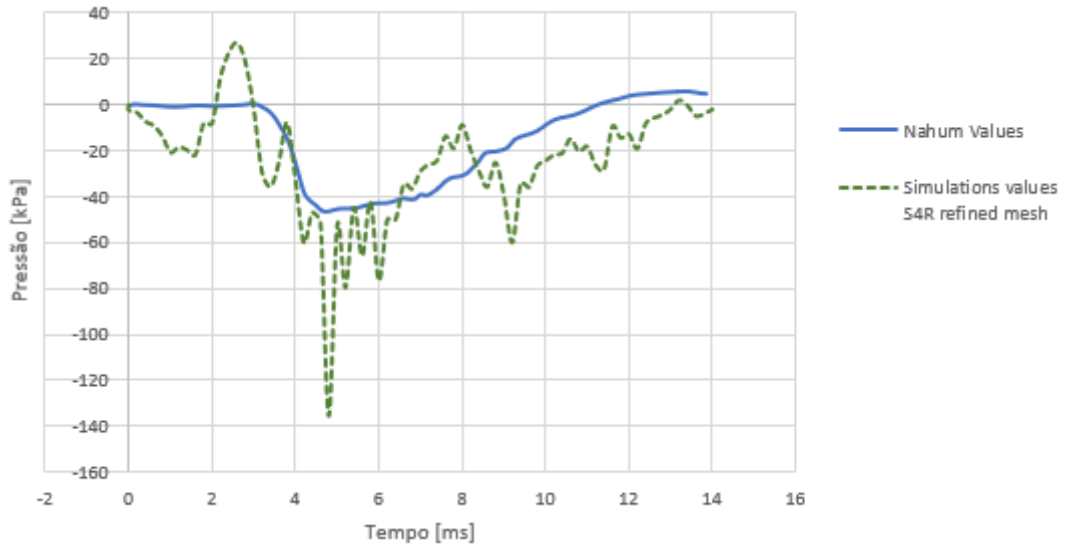

Figure 4.17: Occipital 1 pressure comparison - S4R element with refined mesh

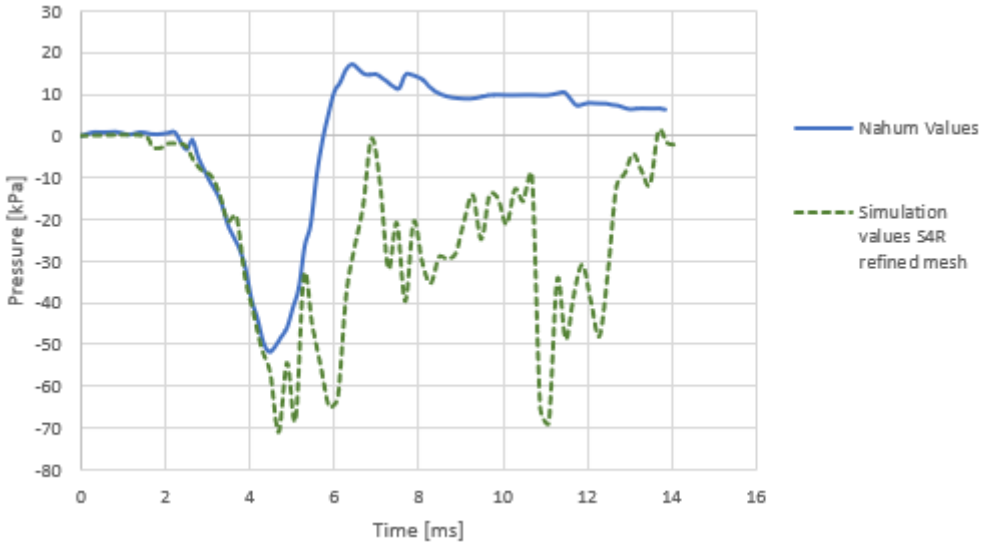

Figure 4.18: Occipital 2 pressure comparison - S4R element with refined mesh

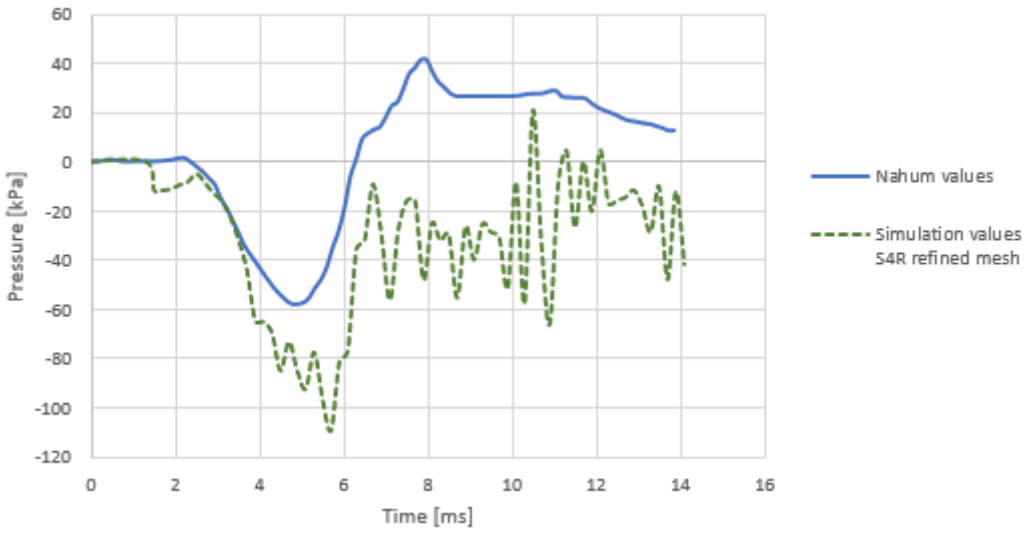

Figure 4.19: Posterior fossa pressure comparison - S4R element with refined mesh

Although the efforts to make this method work none of the meshes nor elements tested were good enough to replace the method employed by Fernandes [9]. The reason for this might be the way this method works.

First it starts with calculating the volume of the cavity using the surface prescribed and the reference point to know the inside. Then, after the impact, it calculates the volume of the deformed cavity and using the bulk modulus and density it is able to extrapolate the pressure values to each element of the surface.

This represents a problem since one of the CSF functions is to support the brain and in

the event of an impact the CSF should act as a cushion absorbing some of the impact energy and then transmit it to the brain [14], a dynamic that this method is unable to reproduce making it an unbiofidelic method to model the skull brain interaction.

The consequences of a poor simulation of this dynamic are the brain being free to move around inside the skull resulting in extreme contact with the dura mater surface making the results oscillate and a misrepresentation of the distribution of the intracranial pressure caused by the CSF motion due the displacement of the brain which ultimately leads to poor results.

4.3 Overall results

In here the overlapped curves obtained are presented all the elements tested are compared.

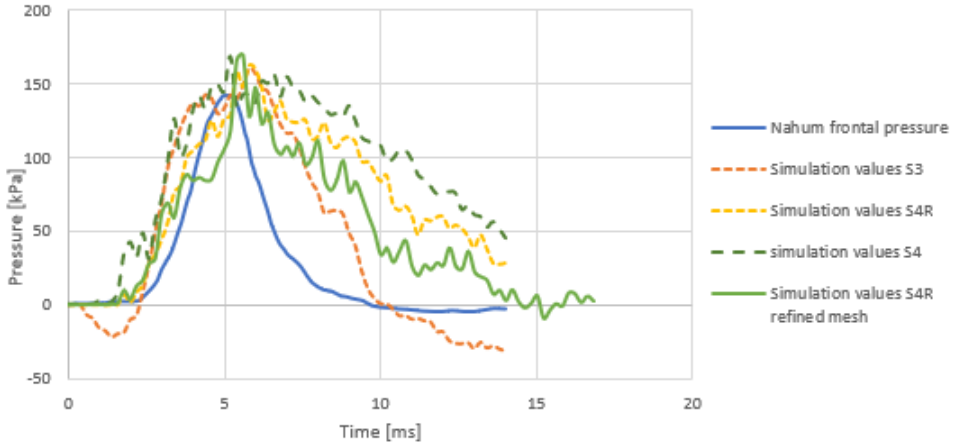

Figure 4.20: Overall frontal comparison
Overall Occipital1 comparison

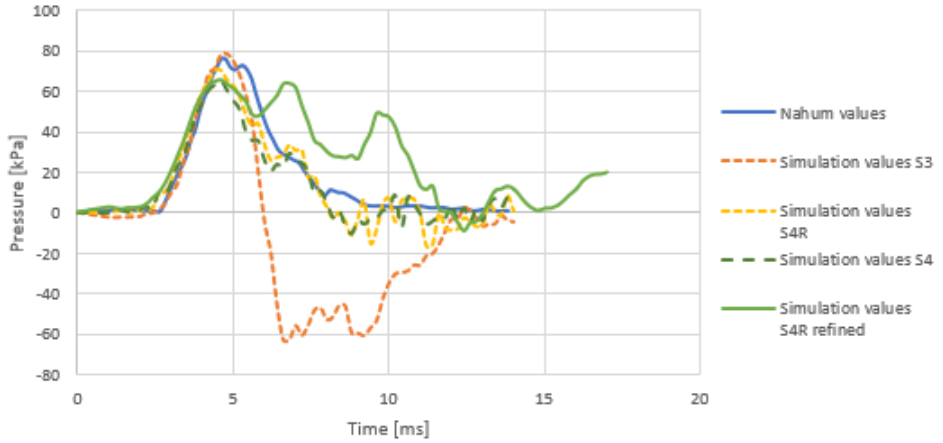

Figure 4.21: Overall parietal comparison

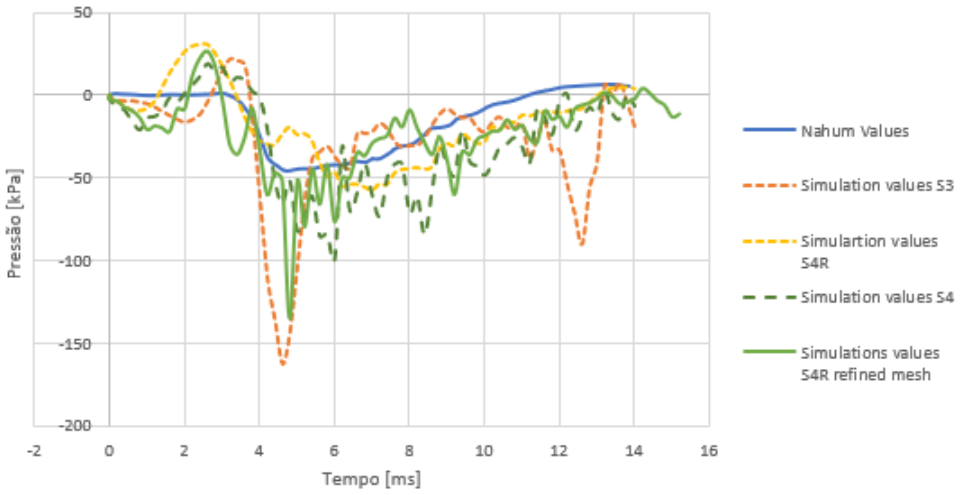

Figure 4.22: Overall Occipital1 comparison

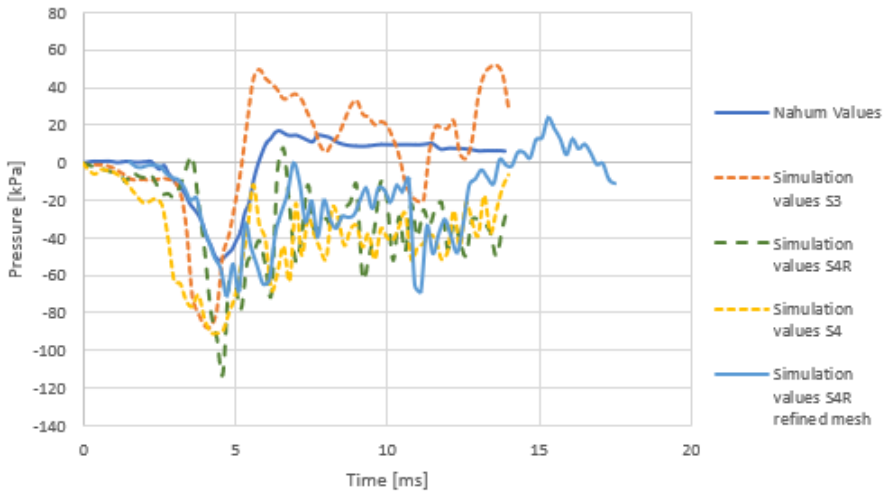

Figure 4.23: Overall Occipital2 comparison

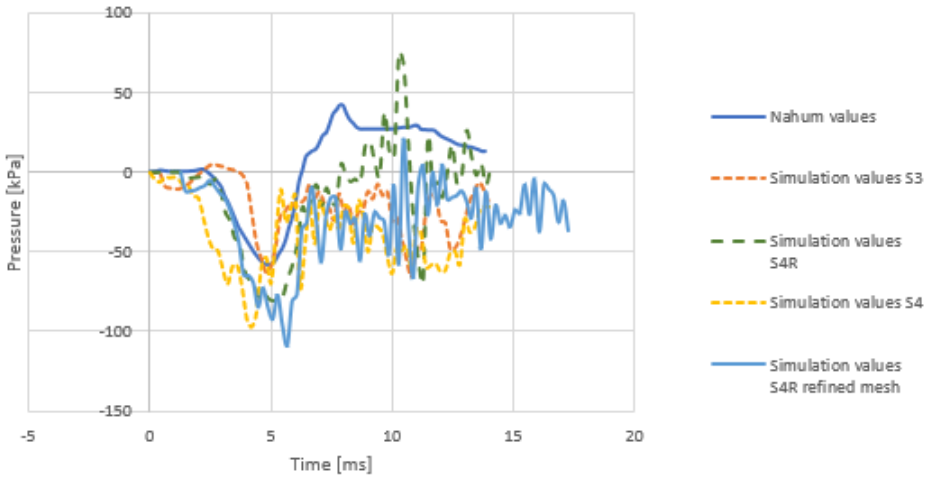

Figure 4.24: Overall Posterior fossa comparison

Chapter 5

Conclusion and future work

Traditionally CSF has been modelled as a solid and then attributed fluid-like properties. This method of discretizing the CSF although practical and computationally efficient has a problem of excessive element distortion which results in inaccuracy in the results obtained hence in the development of this work Abaqus fluid cavity method was used to model the CSF and tested in order to assess its accuracy.

With this purpose in mind literature was reviewed to gain an understanding of the different constituent parts of the human head, how head trauma is assessed and the history of finite element head models and their properties.

To implement this method a dura matter geometry was created and incorporated into the current version of the YEAHM model. Different property values, meshes and elements were simulated to tune the model in order to produce the most accurate as possible results. The results were posteriorly validated against experimental data.

Although at first this method seemed promising since it simplified the complexity while introducing a new part it eventually proved itself to be inaccurate when compared to experimental data due being unable to represent properly the interaction between the brain and skull which consequently made the results less faithful than those achieved with current techniques.

5.1 Future works

The YEAHM already present itself with high level of complexity incorporating several different parts as the skull, brain, CSF, SSS and bridging veins yet there are still other parts that could be included as the falx, arachnoid matter and pia matter are just some of the examples that could be an interesting future development for this model.

Having in consideration the work developed it is also suggested to try to model the CSF with the coupled eulerian lagrangian method or the smooth particle hydrodynamic. Although these methods are extremely complex to implement and computationally costly they offer important advantages such as a method to deal with the severe mesh distortions difficulties due to large deformations in the CFS region and would bring biofidelity to

the model of the interaction between the brain and skull which has been highlighted as of great importance in the precision of the results achieved by FEHMs.

Bibliography

[1] A. Kumar, S. Lalwani, D. Agrawal, R. Rautji, and T. Dogra, "Fatal road traffic accidents and their relationship with head injuries: An epidemiological survey of five years," *Indian Journal of Neurotrauma*, vol. 05, no. 02, pp. 63–67, 2008.

[2] J. X. Jin, J. Y. Zhang, X. W. Song, H. Hu, X. Y. Sun, and Z. H. Gao, "Effect of cerebrospinal fluid modeled with different material properties on a human finite element head model," *Journal of Mechanics in Medicine and Biology*, vol. 15, no. 3, pp. 1–19, 2015.

[3] M. S. Chafi, V. Dirisala, G. Karami, and M. Ziejewski, "A finite element method parametric study of the dynamic response of the human brain with different cerebrospinal fluid constitutive properties," *Proceedings of the Institution of Mechanical Engineers, Part H: Journal of Engineering in Medicine*, vol. 223, no. 8, pp. 1003–1019, 2009.

[4] Physio-pedia, "Classification of Traumatic Brain Injury", Available: https://www.physio-pedia.com/Classification_of_Traumatic_Brain_Injury, Accessed: 2021-04-19."

[5] G. L. Sternbach, "The Glasgow Coma Scale," *Journal of Emergency Medicine*, vol. 19, no. 1, pp. 67–71, 2000.

[6] K. Liesemer, J. Riva-Cambrin, K. S. Bennett, S. L. Bratton, H. Tran, R. R. Metzger, and T. D. Bennett, "Use of Rotterdam CT scores for mortality risk stratification in children with traumatic brain injury," *Pediatric Critical Care Medicine*, vol. 15, no. 6, pp. 554–562, 2014.

[7] F. Tarlochan, "Finite Element (FE) Human Head Models / Literature Review," *Finite Element (FE) Human Head Models / Literature Review*, vol. 2, no. 7, pp. 17–31, 2013.

[8] K. M. Tse, S. P. Lim, V. C. Tan, and H. P. Lee, "A Review of Head Injury and Finite Element Head Models A review of head injury and finite element head models," *American Journal of Engineering, Technology and Society*, vol. 1, no. March 2015, 2014.

[9] F. A. O. Fernandes, R. J. Alves de Sousa, and M. Ptak, "Head Injury Simulation in Road Traffic Accidents," *Springer Briefs in Applied Sciences and Technology*, pp. 25–39, 2018.

[10] A. M. Nahum, R. Smith, and C. C. Ward, "Intracranial pressure dynamics during head impact," *SAE Technical Papers*, 1977.

[11] A. Jindal and S. Mukherji, "World report on road traffic injury prevention," *Medical Journal Armed Forces India*, vol. 61, no. 1, p. 91, 2005.

[12] C. H. Hardy and P. V. Marcal, "Elastic analysis of a skull," *Journal of Applied Mechanics, Transactions ASME*, vol. 40, no. 4, 1973.

[13] V. H. Kenner and W. Goldsmith, "Dynamic loading of a fluid-filled spherical shell," *International Journal of Mechanical Sciences*, vol. 14, no. 9, pp. 557–568, 1972.

[14] W. Wolf, *The Human Nervous System*, vol. 22. Humana Press, sixth ed., 1968.

[15] K. A. Zimmermann, "Nervous System: Facts, Function & Diseases, Accessed 2021-03-22," 2018.

[16] M. Chappell and S. Payne, *The Central Nervous System*, vol. 24. Oxford University Press, Inc, 2020.

[17] S. C. Authors, N. Of, and A. At, *II. Anatomy and physiology*, vol. 19. OpenStax, Rice University, 2013.

[18] M. Clinic, "Anatomy of the Brain", Available: https://mayfieldclinic.com/pe-anatbrain.htm, Accessed: 2021-03-23."

[19] Queensland Brain Institute, "Lobes of the brain", Available: https://qbi.uq.edu.au/brain/brain-anatomy/lobes-brain, Accessed: 2021-03-23."

[20] Lakna, "Difference Between Cerebrum and Cerebral Cortex", Available: https://pediaa.com/difference-between-cerebrum-and-cerebral-cortex/, Accessed: 2021-03-22," 2017.

[21] Q. Government, "Brain Map Frontal Lobes", Available: https://www.health.qld.gov.au/abios/asp/bfrontal, Accessed: 2021-03-23," 2021.

[22] B. J. Baars and N. M. Gage, *Cognition, Brain and Consciousness*. Academic press, Elsevier, second edi ed., 2010.

[23] J. D. Schmahmann and D. N. Pandya, "Parietal Lobe," *Fiber Pathways of the Brain*, pp. 89–142, 2009.

[24] S. Sveinbjornsdottir and J. S. Duncan, "Parietal and Occipital Lobe Epilepsy : A Review," *Epilepsia*, vol. 34, no. 3, pp. 493–521, 1993.

[25] L. Learning, "The Diencephalon", Available: https://courses.lumenlearning.com/boundless-ap/chapter/the-diencephalon/, Accessed: 2021-03-29."

[26] V. Singh, *Textbook of Anatomy - Head, neck and brain*. Reed Elsevier India Private Limited, second edi ed., 2014.

[27] D. E. Lieberman, *The evolution of the human head*. London, England: The belknap press of Harvard University press, 2011.

[28] U. Wolf, M. J. Rapoport, and T. A. Schweizer, "Evaluating the affective component of the cerebellar cognitive affective syndrome," *Journal of Neuropsychiatry and Clinical Neurosciences*, vol. 21, no. 3, pp. 245–253, 2009.

[29] T. U. o. A. a. Birmingham, "What does the spinal cord do?", Available: https://www.uab.edu/medicine/sci/faqs-about-spinal-cord-injury-sci/what-does-the-spinal-cord-do, Accessed: 2021-05-10."

[30] Neupsykey, "Ventricular system", Available: https://neupsykey.com/ventricular-system/, Accessed: 2021-04-12," 2016.

[31] D. N. Irani, *Cerebrospinal fluid in clinical practice*, vol. 4. Saunders, Elsevier, 2009.

[32] J. S. Ruan, "Finite Element Modeling of Direct Head Impact," in *Stapp Car Crash Conference Proceedings*, p. 13, SAE technical papers series, 1993.

[33] C. Zhou, T. B. Khalil, and A. I. King, "A new model comparing impact responses of the homogeneous and inhomogeneous human brain," *SAE transactions*, pp. 2999–3015, 1995.

[34] H. Y. Choi, "Numerical human head model for traumatic injury assessment," *KSME International Journal*, vol. 15, no. 7, pp. 995–1001, 2001.

[35] R. Willinger, H. S. Kang, and B. Diaw, "Three-dimensional human head finite-element model validation against two experimental impacts," *Annals of Biomedical Engineering*, vol. 27, no. 3, pp. 403–410, 1999.

[36] T. J. Horgan and M. D. Gilchrist, "The creation of three-dimensional finite element models for simulating head impact biomechanics," *International Journal of Crashworthiness*, vol. 8, no. 4, pp. 353–366, 2003.

[37] Z. Zong, H. P. Lee, and C. Lu, "A three-dimensional human head finite element model and power flow in a human head subject to impact loading," *Journal of Biomechanics*, vol. 39, no. 2, pp. 284–292, 2006.

[38] H. Mao, L. Zhang, B. Jiang, V. V. Genthikatti, X. Jin, F. Zhu, R. Makwana, A. Gill, G. Jandir, A. Singh, *et al.*, "Development of a finite element human head model partially validated with thirty five experimental cases," *Journal of biomechanical engineering*, vol. 135, p. 111002, 2013.

[39] A. I. King, K. H. Yang, L. Zhang, W. Hardy, and D. C. Viano, "Is head injury caused by linear or angular acceleration," *Proceedings of the International Research Conference on the Biomechanics of Impacts (IRCOBI)*, vol. 12, pp. 1 – 12, 2003.

[40] D. K. Menon, K. Schwab, D. W. Wright, and A. I. Maas, "Position statement: Definition of traumatic brain injury," *Archives of Physical Medicine and Rehabilitation*, vol. 91, no. 11, pp. 1637–1640, 2010.

[41] J. Hopkins, "Traumatic Brain Injury, Available: https://www.hopkinsmedicine.org/health/conditions-and-diseases/traumatic-brain-injury ,Accesed 2021-04-16."

[42] V. T. System, "Major trauma guidelines & education - Victorian state trauma system", Available: https://trauma.reach.vic.gov.au/guidelines/traumatic-brain-injury/introduction, Accessed: 2021-06-18."

[43] K. E. Saatman, A. C. Duhaime, R. Bullock, A. I. Maas, A. Valadka, G. T. Manley, D. Brody, C. Contant, P. Dash, R. Diaz-Arrastia, S. Fertig, A. Gean, C. Goodman, W. Gordon, R. Hayes, R. Hicks, J. Langloi, A. Marmarou, D. Moore, G. Murray, D. Okonkwo, L. Papa, L. Phillips, N. Plesnila, C. Robertson, C. Robertson, J. Sahuquillo, R. Silbergleit, E. Steyerberg, N. Stocchetti, E. Teasdale, G. Teasdale, N. Temkin, H. Thompson, K. Tong, L. Wilson, and D. Wright, "Classification of traumatic brain injury for targeted therapies," *Journal of Neurotrauma*, vol. 25, no. 7, pp. 719–738, 2008.

[44] A. I. Maas, C. W. Hukkelhoven, L. F. Marshall, and E. W. Steyerberg, "Prediction of outcome in traumatic brain injury with computed tomographic characteristics: A comparison between the computed tomographic classification and combinations of computed tomographic predictors," *Neurosurgery*, vol. 57, no. 6, 2005.

[45] C. S. Hill, M. P. Coleman, and D. K. Menon, "Traumatic Axonal Injury: Mechanisms and Translational Opportunities," *Trends in Neurosciences*, vol. 39, no. 5, pp. 311–324, 2016.

[46] BrainLine, "Types of Traumatic Brain Injury", Available: https://www.brainline.org/article/types-traumatic-brain-injury , Accessed: 2021-04-29."

[47] J. G. E. S. S. A. V. P. Allen L. Ho, *Mild traumatic brain injury and concussion terminology and classification.* Elsevier, 2018.

[48] D. W. Bryden, J. I. Tilghman, and S. R. Hinds, "Blast-Related Traumatic Brain Injury: Current Concepts and Research Considerations," *Journal of Experimental Neuroscience*, vol. 13, pp. 7–10, 2019.

[49] Tina Joyce; William Gossman; Martin R. Huecker, "Pediatric Abusive Head Trauma, Accessed 2021-04-09."

[50] A. C. Mckee and D. H. Daneshvar, *The neuropathology of traumatic brain injury*, vol. 127. Elsevier B.V., 1 ed., 2015.

[51] P. Dixit, "A Review on Recent Development of Finite Element Models for Head Injury Simulations," *Archives of Computational Methods in Engineering*, vol. 24, no. 4, pp. 979–1031, 2017.

[52] T. A. Shugar, "Transient Structural Response of the linearSKULL-brain system.," in *Stapp Car Crash Conference Proceedings*, 1975.

[53] J. S. Ruan, T. B. Khalil, and A. I. King, "Finite element modeling of direct head impact," *SAE Technical Papers*, 1993.

[54] L. Zhang, K. H. Yang, R. Dwarampudi, K. Omori, T. Li, K. Chang, W. N. Hardy, T. B. Khalil, and A. I. King, "Recent Advances in Brain Injury Research: A New

Human Head Model Development and Validation," *SAE Technical Papers*, vol. 45, no. November, 2001.

[55] H. S. Kang, R. Willinger, B. M. Diaw, and B. Chinn, "Validation of a 3D anatomic human head model and replication of head impact in motorcycle accident by finite element modeling," in *SAE Technical Papers*, 1997.

[56] R. Nickel and P. Marcal, "In-Vacuo modal dynamic response of the human skull," *Journal of Manufactuting science and engineering*, 1974.

[57] H. S. Chan, "Mathematical model for closed head impact," *SAE transactions*, pp. 3814–3825, 1974.

[58] T. Shugar, "Transient structural response of the linear skull-brain system," in *Proceedings: Stapp car crash conference*, (San Diego, USA), pp. 581–614, 1975.

[59] T. A. Shugar and M. G. Katona, "Development of finite element head injury model," *Journal of the Engineering Mechanics Division*, vol. 101, pp. 223–239, 1975.

[60] C. C. Ward and R. B. Thompson, "The development of a detailed finite element brain model," *SAE Technical Papers*, pp. 3238–3252, 1975.

[61] T. B. Khalil and R. P. Hubbard, "Parametric study of head response by finite element modeling," *Journal of Biomechanics*, vol. 10, no. 2, pp. 119–132, 1977.

[62] R. Hosey, "A homeomorphic finite element model of the human head and neck," *Finite elements in biomechanics*, 1982.

[63] K. Ueno, "Two-dimentional finite element model of the cortical impact method for mechanical brain injury," *Crashworthiness and Occupant Protection in Transportation System. SAME*, vol. 126, pp. 121–147, 1991.

[64] S. Kumaresan and S. Radhakrishnan, "Importance of partitioning membranes of the brain and the influence of the neck in head injury modelling," *Medical and Biological Engineering and Computing*, vol. 34, no. 1, pp. 27–32, 1996.

[65] S. Kleiven and W. N. Hardy, "Correlation of an FE model of the human head with local brain motion-consequences for injury prediction," *Stapp Car Crash Journal*, vol. 46, no. November, p. 513, 2002.

[66] M. B. Structures, *The finite element method in the 1990's*. Springer-Verlag Berlin Heidelberg GmbH, first edit ed., 1991.

[67] L. Zhang, K. H. Yang, and A. I. King, "Comparison of brain responses between frontal and lateral impacts by finite element modeling," *Journal of Neurotrauma*, vol. 18, no. 1, pp. 21–30, 2001.

[68] S. Kleiven, "Evaluation of head injury criteria using a finite element model validated against experiments on localized brain motion, intracerebral acceleration, and intracranial pressure," *International Journal of Crashworthiness*, vol. 11, no. 1, pp. 65–79, 2006.

[69] E. G. Takhounts, R. H. Eppinger, J. Q. Campbell, R. E. Tannous, E. D. Power, and L. S. Shook, "On the Development of the SIMon Finite Element Head Model," *SAE Technical Papers*, vol. 2003-Octob, no. October, pp. 107–133, 2003.

[70] E. G. Takhounts, S. A. Ridella, V. Hasija, R. E. Tannous, J. Q. Campbell, D. Malone, K. Danelson, J. Stitzel, S. Rowson, and S. Duma, "Investigation of Traumatic Brain Injuries Using the Next Generation of Simulated Injury Monitor (SIMon) Finite Element Head Model," *SAE Technical Papers*, vol. 2008-Novem, no. November, 2008.

[71] A. R. L. Barbosa, "Desenvolvimento de um modelo computacional do crânio humano Development of a computational model of the human skull," 2020.

[72] D. Systèmes, "Modeling fluid-filled cavities", Available: https://classes.engineering.wustl.edu, Accessed: 2021-03-23."

[73] T. Henderson, "Cerebrospinal Fluid Pressure," *British Medical Journal*, vol. 1, no. 4818, p. 1049, 1953.

[74] D. Systemes, "Explicit dynamic analysis", Available: https://abaqus-docs.mit.edu/2017/English/SIMACAEANLRefMap/simaanl-c-expdynamic.htm, Accessed: 2021-10-07," 2017.

[75] G. Reader, "Graph reader", Available: http://www.graphreader.com/, Accessed 2021-10-07."